PARAMETRIC CYCLE ANALYSIS

FOR PULSE DETONATION ENGINES

by

HAIDER HEKIRI

Presented to the Faculty of the Graduate School of

The University of Texas at Arlington in Partial Fulfillment

of the Requirements

for the Degree of

MASTER OF SCIENCE IN AEROSPACE ENGINEERING

THE UNIVERSITY OF TEXAS AT ARLINGTON

December 2005

ACKNOWLEDGEMENTS

I would like to take this opportunity to acknowledge the individuals at the University of Texas at Arlington who have helped reach this milestone in my life. My supervising professor Dr. Frank Lu, in spite of his busy schedule, took me under his wings and gave me the chance to work with him on such an interesting research. He was very helpful at all times as he maintained an ever-standing "open door" policy to help keep students such as myself on track and focused on the tasks at hand by providing insight, advice, and academic support as well as the ambition to explore new ideas and concepts in propulsion and, in particular, pulse detonation engines.

Dr. Wilson taught me the basics of propulsion and made me enjoy researching further on this subject; he was very encouraging and very helpful whenever he was available. I would also like to thank the AIAA student chapter at UTA. The student organization has served as a cornerstone and a focal point for students sharing a common goal and similar interests. Through students helping students, shared achievements have forged friendships that will last a lifetime.

November 21, 2005

ABSTRACT

PARAMETRIC CYCLE ANALYSIS

FOR PULSE DETONATION ENGINES

Publication No. _____

Haider Hekiri, MS

The University of Texas at Arlington, 2004

Supervising Professor: Dr. Frank Lu

The performance of an ejector-driven pulse detonation engine (PDE) with an afterburner is analytically estimated. In the analysis, the PDE was modeled as a straight tube, closed at the front end and open at the other. A detonation wave starts to travel after it is ignited at the closed end, causing a Chapman-Jouguet detonation wave followed by a Taylor rarefaction to travel to the open end. At that point, rarefaction waves are reflected back to the closed end. The result is a high thrust due to both the primary and secondary flows of the ejector-driven PDE. A theoretical analysis is made to determine the average thrust density and the impulse density per cycle of the primary

flow. The mixed flow of the PDE tube and the ejector is then subjected to afterburning. The overall engine performance was eventually derived.

TABLE OF CONTENTS

LIST OF ILLUSTRATIONS

Figure Page

CHAPTER 1

INTRODUCTION

There are two types of rocket engine combustion. The first is deflagration. In this process, the flame from the fuel-oxidizer mixture travels at a slow rate, typically a few meters per seconds. The second type of combustion, which is the focus of our analysis, is detonation combustion where a detonation wave is propagated into the fuel/oxidizer mixture. The wave travels at a speed of a few thousand meters per seconds, compressing the fluid in front of it, increasing its density, pressure and therefore temperature, thereby, causing the initiation of chemical reactions. The Chapman-Jouguet (CJ) detonation wave comprises of a shock wave closely coupled to a thin flame front. The high pressure produced by the detonation without the use of a compressor has led to proposals for various propulsion devices based on detonations. Recently, pulse detonation engine (PDE) technology has received a great deal of consideration due to its potential for producing thrust with greater efficiency than turbomachinery-based engines where the fuel is burned by deflagration.

1.1 Chapman-Jouguet Model

In thermodynamic analysis, it is usual to model a PDE using a Humphrey cycle, as opposed to a Brayton cycles for conventional, deflagration-based propulsion systems. In a Brayton cycle, the process of heat addition depends on constant pressure combustion (leg 2-5) in Figure 1.1. However, for the Humphrey cycle, this constant pressure heat addition process is replaced by constant volume combustion (leg 2-3).

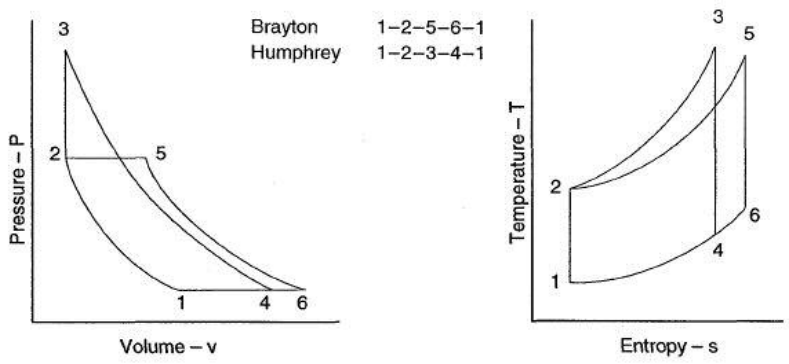

Figure 1.1 Pressure-volume and temperature-entropy graphs for the constant volume combustion Humphrey and constant pressure Brayton cycles.

A cycle, known as the detonation cycle, similar to the Brayton cycle, can be seen as part of the reactive Hugoniot curve in Figure 1.2. In the reactive Hugoniot curve there are five regions. Regions I and IV are for strong detonation and deflagration respectively, while regions II and V are for weak detonation and deflagration respectively. Region III is physically impossible. The final state of either a deflagration or a detonation is located on both the Rayleigh line and the reactive Hugoniot curve so that conservation conditions are satisfied. Points B and E in Figure 1.2 are those points that respectively represent the upper and the lower CJ locations.

The lower CJ location represents the separation of the strong and the weak deflagration region. The speed at that point is the CJ deflagration velocity. The upper CJ location (point B) represents the separation of the strong and the weak detonation region. The velocity of the detonation at that region is the same as the speed of sound of the products. This upper CJ point corresponds to the steady end condition of the detonation wave. The upper branch of the reactive Hugoniot shown in Figure 1.2 is the main concern of this work.

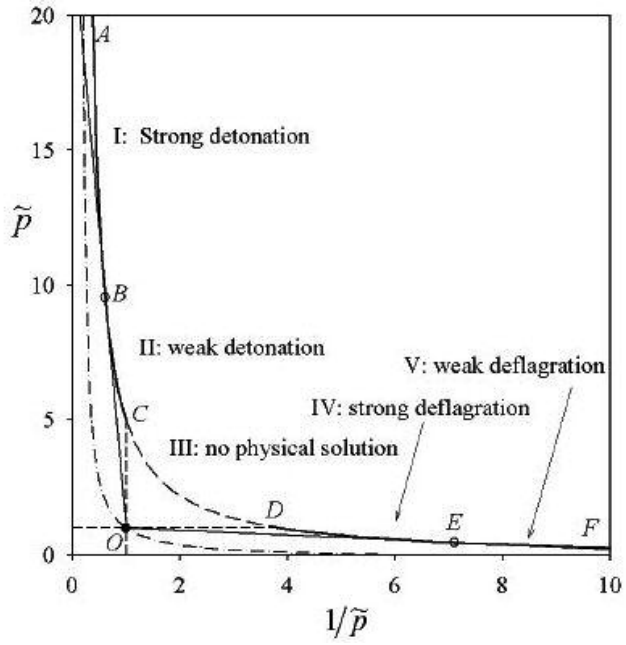

Figure 1.2 Various combustion regimes. Inert hugoniot is shown as dashed dotted line Hugoniot with heat addition is shown as solid line.

1.2 Pulse Detonation Cycle Overview

A pulse detonation (PD) device consists of a detonation combustion chamber coupled with a propellant feed system. The feed system hardware is an important component in the PD device. It includes fuel and oxidizer pumps, gas generators, ducting and valves. Other components are precise flow metering valves which allow steady manifold flow, and detonation initiation systems. The main component of the PD device is the detonation tube where the combustion takes place, and the cooling system that keeps the detonation combustor at relatively low temperature.

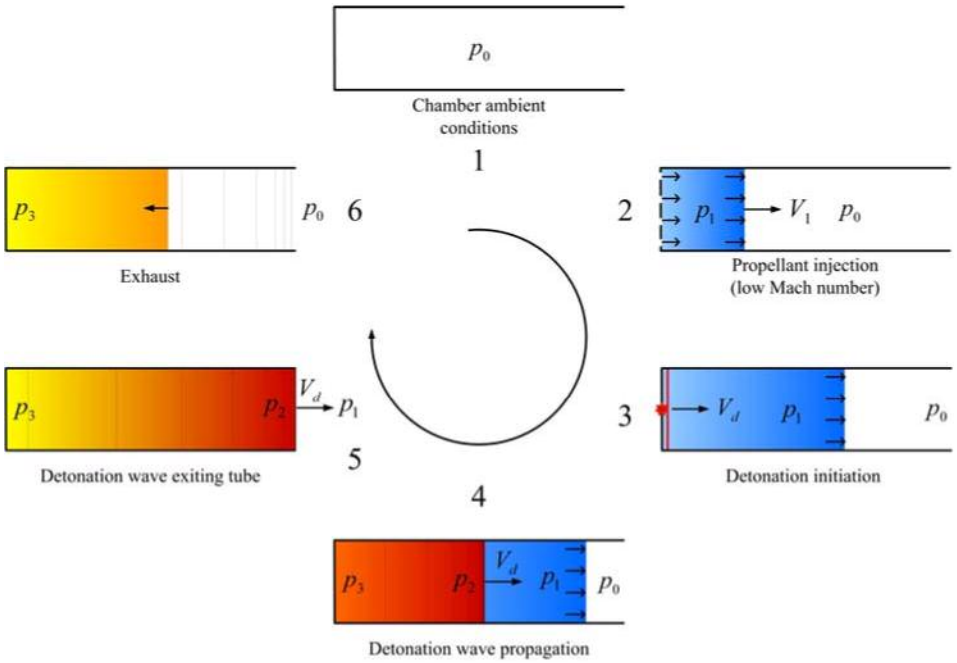

Figure 1.3 Basic scheme of a pulse detonation cycle.

A PDE cycle is shown schematically in Figure 1.3. The cycle consists of several distinct events. Starting with the detonation chamber which just expelled the product of

the previous cycle and is ready for re-charging (1), a valve is opened and the combustion chamber is filled with a fuel/oxidizer mixture (2). A valve seals the detonation chamber and the detonation initiator ignites the propellant mixture causing a detonation to form at the closed end of the detonation tube (3). The detonation wave propagates through the chamber (4) and exits the combustion chamber, generating a series of rarefaction waves at the open end (5). The rarefaction waves travel from the open end to the closed end, causing the burned gas to exhaust (6). The pressure in the combustion chamber drops and the chamber is ready for re-charging (1). Usually, air is used to purge the tube off hot detonation products, so as to prevent them from igniting the incoming fresh propellant mixture for the next cycle. The cycle time can regarded as the sum of four processes, namely, the purge, fill, detonation and rarefaction processes:

$$T_{cycle} = t_{purge} + t_{fill} + t_{detonation} + t_{rarefaction}$$

The representation of the PD cycle in the reactive Hugoniot curve and the Rayleigh line shown in Figure 1.2 can be followed by tracking the path OBDO, where O-B is the detonation path, B-D is the expansion and the exhaust of the burned gas, and D-O is the constant pressure return to the initial state. The same process can be shown in the pressure-volume and temperature-entropy graph in Figure 1.1 by following the path 1-2-3-4-1.

In the next chapter, an analysis of an ejector-driven PDE will be provided. The system operates as a replacement for a high-pressure compressor and a high-pressure turbine, thus yielding a potential reduction in cost due to the elimination of those

turbomachinery components. In addition, reductions in engine weight and improvement in the engine fuel consumption are other benefits of eliminating the compressor and the turbine. The goal of this study is to illustrate the possible thrust augmentation with an ejector-driven PDE and therefore it provides a theoretical basis that can possibly help improve the performance of this new technology.

Initially, the performance of a basic pulse detonation engine without an ejector is analytically estimated by using a simple model of a single tube combustion chamber PDE. A simplified theoretical analysis for the CJ detonation wave, the impulse density and the time-averaged thrust density per cycle is derived. A subsequent analysis is made to take the ejector into account, where several mixing flow properties are examined and mixing pressure and temperature are calculated. Finally, an afterburner is added at the end of the mixing shroud. The exit pressure, temperature and flow speed, and efficiencies are calculated. Therefore the performance of the ejector-driven PDE is obtained.

CHAPTER 2

ANALYTICAL METHOD FOR EJECTOR PDE

2.1 Single detonation tube analysis

The goal of this step is to derive the average thrust density as well as other performance parameters of a basic PDE. This derivation includes local gas properties such as pressure, density, local velocity and waves travel time (p, ρ, V, t). The total cycle time T_{cycle} and the impulse density I_{cycle} are also calculated. Therefore, the average thrust density $p_{average}$ is found.

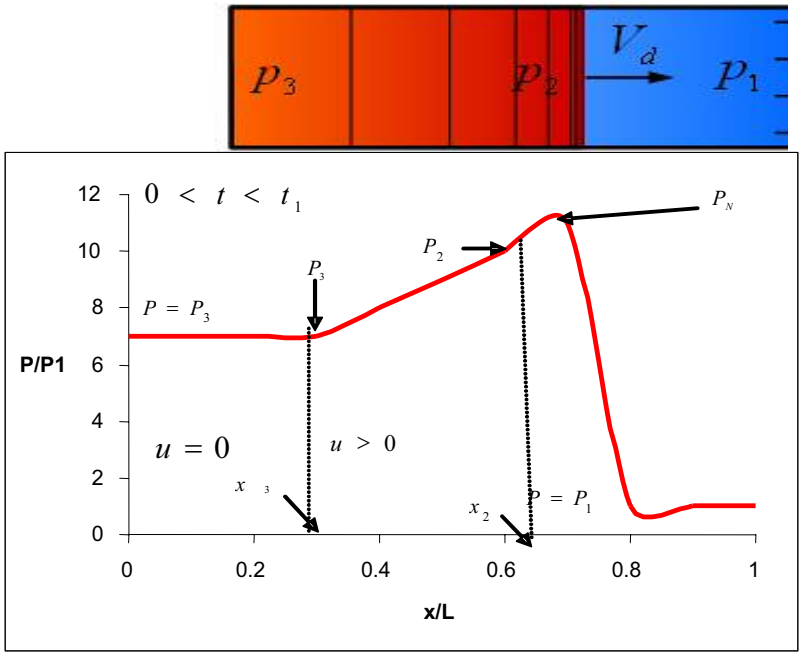

Figure 2.1 Pressure distribution at instant $0 < t < t_1$

The cycle analysis time starts when the propellant mixture fills the combustion chamber, and the igniter initiates the detonation wave. This is illustrated in Figure 2.1 which shows the pressure distribution at $0 < t < t_1$, where t_1 is the time for the CJ wave to exit the detonation chamber. Initially, the local gas properties and conditions of the unburned detonable mixture have the values of p_1, ρ_1, γ_1. The velocity u_1 of the detonable mixture is initially equal to zero.

At the beginning of cycle, at t = 0, the detonation mixture is ignited and the CJ detonation wave starts to propagate to the right into the open end. At the front end of the detonation wave is the von Neumann spike behind which chemical reactions occur. Due to the heat release q from the reactions, the gas properties of the von Neumann spike are obtained via [1]:

$$\rho_N = \frac{\gamma_1 + 1}{\gamma_1 - 1}\rho_1 \tag{1}$$

$$p_N = \frac{2\gamma_1}{\gamma_1 + 1}M_{CJ}^2 p_1 \tag{2}$$

where M_{CJ} is the Mach number of the CJ wave, the subscript 1 is for the undisturbed gas property and the subscript 2 refers to properties downstream of the CJ wave. The speed of the CJ wave

$$D_2 = D_{CJ} = \sqrt{2(\gamma_2{}^2 - 1)q} \tag{3}$$

The pressure and density of the CJ wave are given by

$$p_2 = \frac{\gamma_2 + 1}{\gamma_2} M_{CJ}{}^2 p_1 \tag{4}$$

$$\rho_2 = \frac{\gamma_2 + 1}{\gamma_2} \rho_1 \tag{5}$$

The velocity of the CJ wave is

$$u_2 = \frac{1}{\gamma_2} a_2 = \frac{1}{\gamma_2 + 1} D_{CJ} \tag{6}$$

The distance of the CJ detonation from the closed end is

$$x_2 = D_2 t = D_{CJ} t \tag{7}$$

The rightmost boundary of the rarefaction wave facing the CJ detonation has the same gas state as the CJ wave

$$\begin{aligned} p &= p_2 \\ \rho &= \rho_2 \\ u &= u_2 \\ D &= D_2 \end{aligned} \tag{8}$$

The left most boundary side has the same gas properties as the burned gas at rest. This boundary is assumed by [1] to be half of the CJ distance, which is in (Fig. 2.1)

$$x_3 = \frac{x_2}{2} \tag{9}$$

The speed of the leftmost boundary is therefore equal to

$$D_3 = \frac{D_{CJ}}{2} \tag{10}$$

The gas density and pressure of the burned gas at rest is given by [1]

$$\rho_3 = 2\left(\frac{\gamma_2+1}{2\gamma_2}\right)^{\frac{\gamma_2+1}{\gamma_2-1}}\rho_1 \tag{11}$$

$$p_3 = \frac{\gamma_1}{2\gamma_2}\left(\frac{\gamma_2+1}{2\gamma_2}\right)^{\frac{\gamma_2+1}{\gamma_2-1}} M_{CJ}{}^2 p_1 \tag{12}$$

The state of the gas in between the two sides of the rarefaction wave is a nonlinear function of the distance x where $x_3 < x < x_2$ in Figure 2.1. The relation of the gas properties in this region is given by

$$p = \left(\frac{1}{\gamma_2} + \frac{\gamma_2-1}{\gamma_2}\frac{x}{x_2}\right)^{\frac{2\gamma_2}{\gamma_2-1}} p_2 \tag{13}$$

$$\rho = \left(\frac{1}{\gamma_2} + \frac{\gamma_2-1}{\gamma_2}\frac{x}{x_2}\right)^{\frac{2}{\gamma_2-1}} \rho_2 \tag{14}$$

The local velocity and sonic speed of the gas inside the rarefaction is a function of the distance x and time t by

$$a = a_2 - \frac{\gamma_2-1}{\gamma_2+1}\frac{x_2-x}{t} \tag{15}$$

$$u = u_2 - \frac{2}{\gamma_2+1}\frac{x_2-x}{t} \tag{16}$$

When the CJ wave and Taylor rarefaction exit the tube, the gas is assumed to be at a uniform condition and at rest within the tube.

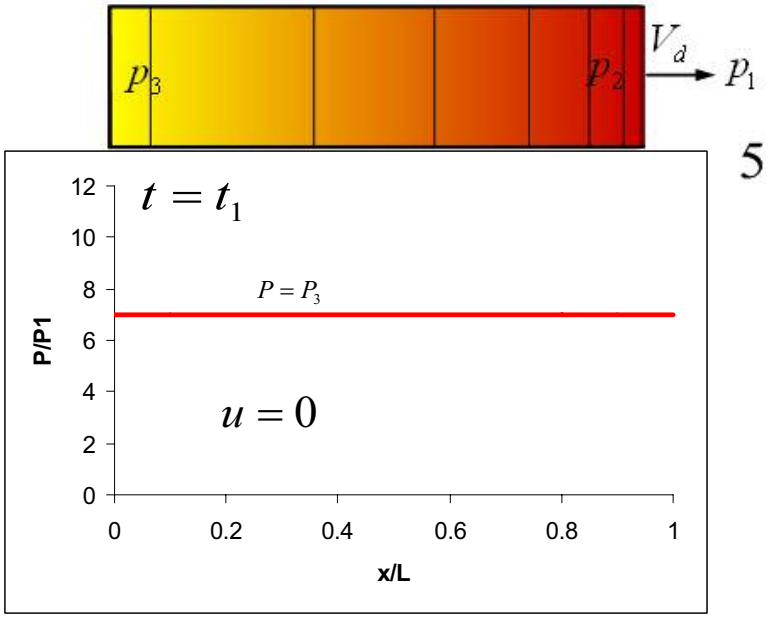

Figure 2.2 Pressure distribution at instant $t = t_I$.

The estimation of the exit time t_I is found by dividing the tube length over the rarefaction travel speed.

$$t_I = \frac{L}{D_3} = \frac{2L}{D_{CJ}} \tag{17}$$

At that instance, another rarefaction starts to propagate from the open end to the closed end as shown in Figure 2.3, causing the burned gas to exhaust at the open end of the tube. This rarefaction wave reaches the closed end at $t = t_{II}$.

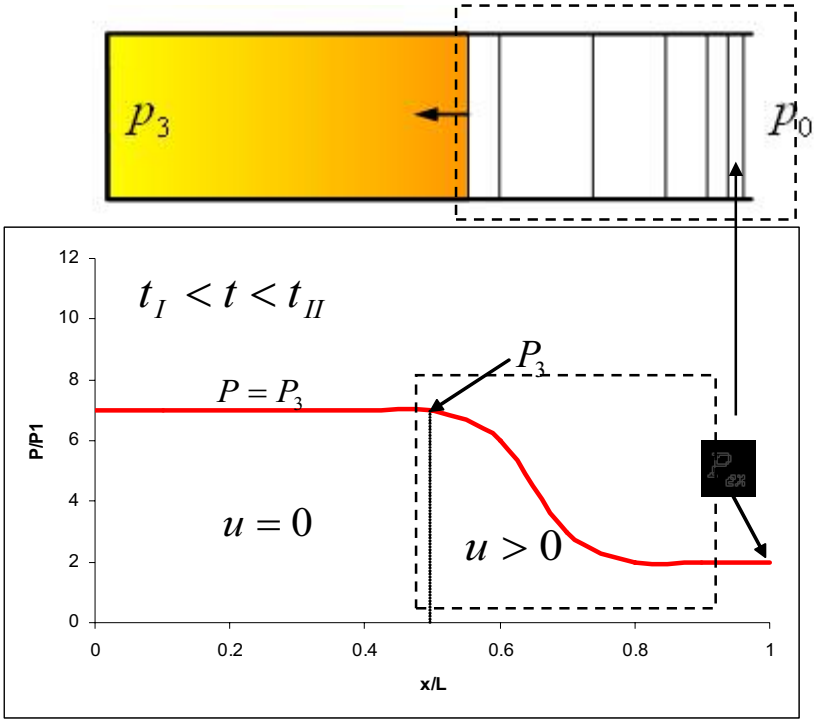

Figure 2.3 Pressure distribution at instant $t_I < t < t_{II}$.

The leftmost boundary of this wave has the same properties of the gas at rest inside the tube. However the state of the gas inside the wave is a function of the exhausted gas [1,2] where

$$p_{ex} = \frac{\gamma_1}{\gamma_2^{\frac{2\gamma_2}{\gamma_2-1}}(\gamma_2+1)} M_{CJ}{}^2 p_1 \tag{18}$$

$$\rho_{ex} = \frac{\gamma_2+1}{\gamma_2^{\frac{\gamma_2+1}{\gamma_2-1}}} \rho_1 \tag{19}$$

$$u_{ex} = a_{ex} = \frac{1}{\gamma_2+1} D_{cj} \tag{20}$$

Similar to the CJ detonation equations, the gas pressure, density, velocity and sonic speed are

$$p = \left(1 + \frac{\gamma_2 - 1}{D_{CJ}} \frac{L - x}{t - t_I}\right)^{\frac{2\gamma_2}{\gamma_2 - 1}} p_{ex} \tag{21}$$

$$\rho = \left(1 + \frac{\gamma_2 - 1}{D_{CJ}} \frac{L - x}{t - t_I}\right)^{\frac{2}{\gamma_2 - 1}} \rho_{ex} \tag{22}$$

$$u = u_{ex} - \frac{2}{\gamma_2 + 1} \frac{L - x}{t - t_1} \tag{23}$$

$$a = a_{ex} - \frac{\gamma_2 - 1}{\gamma_2 + 1} \frac{L - x}{t - t_I} \tag{24}$$

The time required for the rarefaction wave to travel from the open to the closed end is

$$t_{II} - t_I = \frac{L}{a_3} = \frac{2L}{D_{CJ}} \tag{25}$$

$$t_{II} = \frac{2L}{D_{CJ}} + t_I = \frac{4L}{D_{CJ}} \tag{26}$$

The time for the burned gas to completely exit the detonation tube is $t = t_{III}$ and the time from when the rarefaction wave starts to propagate back till the gas completely exits the tube, that is $t_I < t < t_{III}$, is called the exhaust phase. The value of t_{III} can be found from dividing the mass of the burned gas inside the tube by the mass flow rate of that gas when it exits

$$t_{III} = \frac{m_3}{\dot{m}_{ex}} + t_I \tag{27}$$

The mass of the gas per unit area inside the tube is defined by

$$m_3 = \rho_3 L \tag{28}$$

The exhausted gas mass flow rate per unit area according to [1] is given by

$$\dot{m}_{ex} = \rho_{ex} u_{ex} = \frac{2^{\frac{2}{\gamma_2 - 1}}}{(\gamma_2 + 1)^{\frac{\gamma_2 + 1}{\gamma_2 - 1}}} D_{CJ} \rho_3 = \left(\frac{2}{\gamma_2 + 1} \right)^{\frac{\gamma_2 + 1}{\gamma_2 - 1}} \rho_3 a_3 \tag{29}$$

Therefore the value of t_{III}

$$t_{III} = \frac{\rho_3 L}{\rho_{ex} u_{ex}} + t_I \tag{30}$$

Solving the previous equation, we get the full exhaust time

$$t_{III} = \left[1 + \left(\frac{\gamma_2 + 1}{2} \right)^{\frac{\gamma_2 + 1}{\gamma_2 - 1}} \right] \frac{2L}{D_{CJ}} \tag{31}$$

Experiments on PDE show that during the purging time, there is more than one Taylor rarefaction wave travels from the open end to the closed end of the tube. Those waves form a fan of straight lines; those lines are the characteristic lines. With increasing time the fan becomes wider, or in other word, the wave becomes "flatter", and the gradients of velocity and density become smaller. As a result, equation (30) for t_{III} will have a smaller value, since ρ_3 during the exhaust is decreasing. The variation of ρ_3 can be obtained using the method of characteristics [3]. However, for analytical simplicity, ρ_3 in this analysis is assumed to be constant.

The time required to completely purge the remaining hot products from the detonation tube is t_{purge}, the purge time which can be regarded to be of the same order of magnitude as the filling time t_{fill}. They are both related to the tube length. Thus, in this

analysis the purge time t_{purge} is set to be equal to the filling time t_{fill} . The period of a PDE cycle T_{cycle} is thus

$$T_{cycle} = t_{III} + t_{purge} + t_{fill} \tag{32}$$

Substituting equation (31) for t_{III} into equation (32), we get the full cycle time

$$T_{cycle} = \left[1 + \left(\frac{\gamma_2 + 1}{2} \right)^{\frac{\gamma_2 + 1}{\gamma_2 - 1}} \right] \frac{2L}{D_{CJ}} + t_{purge} + t_{fill} \tag{33}$$

The PDE cycle frequency can then be derived as

$$f_{cycle} = \frac{1}{T_{cycle}} = \frac{1}{\left[1 + \left(\frac{\gamma_2 + 1}{2} \right)^{\frac{\gamma_2 + 1}{\gamma_2 - 1}} \right] \frac{2L}{D_{CJ}} + t_{purge} + t_{fill}} \tag{34,35}$$

The thrust density of the PDE is given by

$$P_{ave} = \frac{I_{cycle}}{T_{cycle}} \tag{36}$$

where I_{cycle} is the impulse density acting on the thrust wall for one cycle. The impulse density is the time integration of the pressure distribution at the thrust wall during the full cycle time, namely,

$$I_{cycle} = \int_0^{T_{cycle}} p_w(t) dt \tag{37}$$

It has been described earlier that the pressure at the thrust wall p_w changes with each cycle phase. At the beginning of the cycle until the second rarefaction wave

reaches the closed end, that is $0 \le t \le t_{II}$, the pressure at the wall is equal to p_3. Then, from the time at which the second rarefaction wave reaches the closed end until the full purging time, that is $t_{II} \le t \le t_{III}$, the pressure distribution at the wall will decrease as follows [1]

$$p_w(t) = p_3\left(1 - \frac{t - t_{II}}{t_{III} - t_{II}}\right) \tag{38}$$

For the rest of the cycle time, $t_{III} \le t < T_{cycle}$ the pressure is equal to zero [1]. Therefore, the integral equation of the impulse density can be written as:

$$I_{cycle} = \int_0^{t_{II}} p_3 dt + \int_{t_{II}}^{t_{III}} p_3\left(1 - \frac{t - t_{II}}{t_{III} - t_{II}}\right)dt + \int_{t_{III}}^{T_{cycle}} 0 dt \tag{39}$$

where

$$p_3 = \frac{\gamma_1}{2\gamma_2}\left(\frac{\gamma_2 + 1}{2\gamma_2}\right)^{\frac{\gamma_2+1}{\gamma_2-1}} M_{CJ}^2 p_1 \tag{40}$$

Integrating equation (39) with respect to time yields

$$I_{cycle} = \frac{1}{2\gamma_2}\left(\frac{\gamma_2 + 1}{2\gamma_2}\right)^{\frac{\gamma_2+1}{\gamma_2-1}}\left[3 + \left(\frac{\gamma_2 + 1}{2}\right)^{\frac{\gamma_2+1}{\gamma_2-1}}\right]\rho_1 D_{CJ} L \tag{41}$$

Having the equations for the impulse density I_{cycle} and the total cycle time of the tube T_{cycle}, the equation of the average thrust density can be assembled as follows:

$$P_{ave} = \frac{I_{cyc}}{T_{cyc}} \tag{43}$$

$$\therefore P_{ave} = \frac{\dfrac{1}{2\gamma_2}\left(\dfrac{\gamma_2+1}{2\gamma_2}\right)^{\frac{\gamma_2+1}{\gamma_2-1}}\left[3+\left(\dfrac{\gamma_2+1}{2}\right)^{\frac{\gamma_2+1}{\gamma_2-1}}\right]\rho_1 D_{CJ} L}{\left[1+\left(\dfrac{\gamma_2+1}{2}\right)^{\frac{\gamma_2+1}{\gamma_2-1}}\right]\dfrac{2L}{D_{CJ}} + t_{purge} + t_{fill}} \tag{44}$$

2.2 Performance analysis with an ejector and afterburner

The goal of this step is to determine the engine performance when an ejector and an afterburner are added as part of the PDE. The equations for the specific thrust, specific fuel consumption and the thermal and propulsive efficiencies are derived. Starting from the inlet plane of the ejector shroud, the analysis can be treated as a special case of a turbojet cycle, where the compressor pressure ratio π_c is replaced by the ejector pressure ratio π_{ejec}. The turbine section is eliminated. Having all the values of the turbojet cycle analysis adjusted, the performance analysis of the ejector-driven PDE is ready to be carried out, where some assumptions are taken for simplicity.

A schematic of the ejector-driven PDE is given in Figure 2.4. The figure shows the high-pressure primary flow produced by the PDE detonation tube interacting with the secondary flow that arrives from the ejector inlet. The primary flow raises the secondary flow's total pressure from an ambient condition pressure to an intermediate value. The static and total pressures at the ejector exit are found here using the

conservation of energy and mass equations. According to reference [4] the static pressure ratio is given by

$$\frac{P_e}{P_0} = (1+\alpha)\frac{A_p}{A}\frac{P_{tp}}{P_0}\sqrt{\frac{T_e}{T_{tp}}}\left(\frac{2}{1+\gamma}\right)^{\frac{\gamma+1}{2(\gamma-1)}} \tag{45}$$

where α is the bypass ratio, P_{tp} is the cycle average detonation pressure P_{ave} found on equation (44), A_p/A is the tube-to-shroud area ratio, T_e/T_{tp} is the ejector-static-to-primary-total pressure ratio and it is given by

$$\frac{T_e}{T_{tp}} = \frac{\gamma-1}{2}\left(\frac{1+\alpha\dfrac{T_{ts}}{T_0}\dfrac{T_0}{T_{tp}}}{1+\alpha}\right) \tag{46}$$

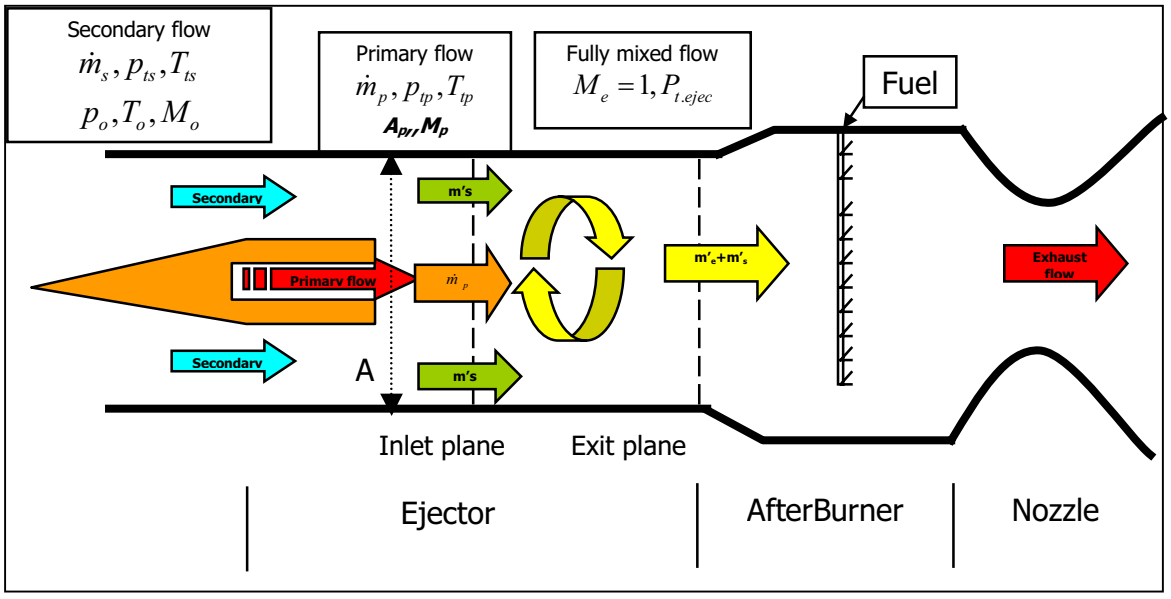

Figure 2.4 Ejector-driven PDE engine.

The bypass ratio $\alpha = \dot{m}_s / \dot{m}_p$ is the ratio of the secondary-to-primary mass flow rate, and it is given by [2]

$$\alpha = \frac{P_{ts}}{P_0}\frac{P_0}{P_{tp}}\frac{A_{si}}{A}\frac{A}{A_{pi}}\frac{M_{si}}{M_{pi}}\sqrt{\frac{T_{tp}}{T_0}\frac{T_0}{T_{ts}}}\left\{\frac{1+\frac{\gamma-1}{2}M_{pi}^{\ 2}}{1+\frac{\gamma-1}{2}M_{si}^{\ 2}}\right\}^{\frac{\gamma+1}{2(\gamma-1)}} \tag{47}$$

where P_{ts}/P_0 and T_{ts}/T_0 are the total pressure and temperature ratios of the secondary flow. Their values are found using the isentropic flow relation with the Mach number as follows:

$$\frac{T_{ts}}{T_0} = 1 + \frac{\gamma-1}{2}M_0^2 \tag{48}$$

$$\frac{P_{ts}}{P_0} = \left(\frac{T_{ts}}{T_0}\right)^{\frac{\gamma}{\gamma-1}}\frac{P_{ts}}{P_{t0}} \tag{49}$$

Now, P_{ts}/P_{t0} is the pressure loss across the engine diffuser π_d. The value for π_d is given from the following equation

$$\pi_d = \pi_{d\max}\eta_r \tag{50}$$

The value of $\pi_{d\max}$ depends on the engine configuration and the level of technology [4]. For supersonic aircraft with engine in airframe and using a level of technology 4 $\pi_{d\max} = 0.96$; η_r is the total pressure recovery of the supersonic inlet, where [4]

$$\eta_r = \begin{cases} 1 & M_0 \le 1 \\ 1 - 0.075(M_0 - 1)^{1.35} & 1 < M_0 < 5 \\ \dfrac{800}{M_0^4 + 0.35} & 5 < M_0 \end{cases} \tag{51}$$

The primary and secondary inlet Mach numbers, M_{pi} and M_{si}, are functions of the recently found pressure ratios [2] and they are given by

$$M_{pi} = \left\{ \frac{1}{\gamma - 1} \left[\left(\frac{P_{tp}}{P_0} \frac{P_0}{P_i} \right)^{\frac{\gamma - 1}{\gamma}} - 1 \right] \right\}^{\frac{1}{2}} \tag{52}$$

$$M_{si} = \left\{ \frac{1}{\gamma - 1} \left[\left(\frac{P_{ts}}{P_0} \frac{P_0}{P_i} \right)^{\frac{\gamma - 1}{\gamma}} - 1 \right] \right\}^{\frac{1}{2}} \tag{53}$$

where according to [2], $P_0 / P_i \approx 1.1$ and $\gamma = 1.35$

The value of the bypass ratio should also include an increased value $\Delta\alpha$ due to the extra entrainment due to the unsteady ejector effect from the PDE core. The unsteady flow from the PDE tends to increase the amount of the secondary flow pulled from the inlet. This is due primarily to the structure of starting a vortex type flow just before the mixing region [6]. The entrainment in the bypass ratio of the steady and the unsteady components of the flow can be found by adding the two values together, that is,

$$\alpha_n = \alpha_{ss} + \alpha_{us} \tag{54}$$

where $\alpha_{ss} = \alpha$ found from equation (47), and α_{us} is the bypass entrainment due to flow unsteadiness. The value of α_{us} is function the ejector area ratio and it is found from a curve fit to experimental data found in reference [6] and shown in Figure 2.5.

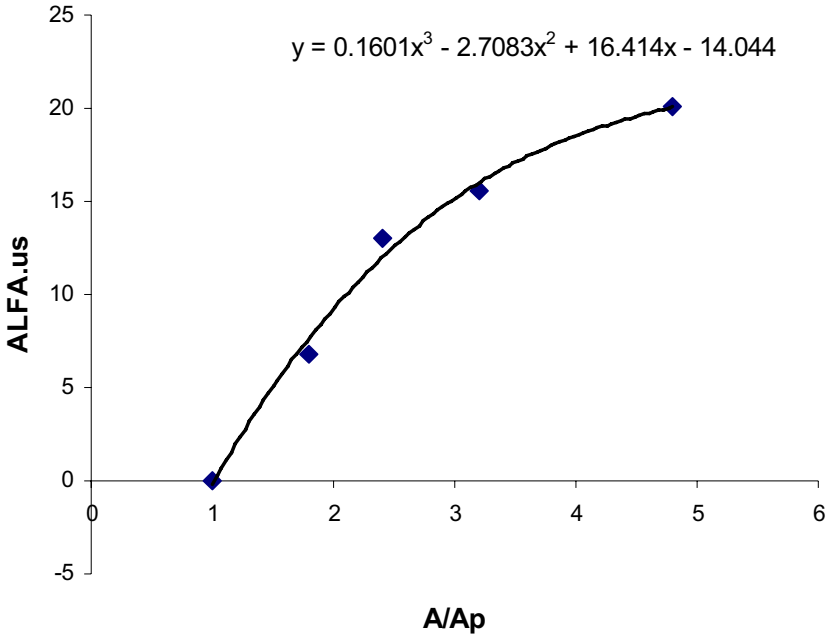

Figure 2.5 Bypass ratio entrainment due to unsteady flow, versus ejector area ratio.

From the fitted curve,

$$\alpha_{us} = 0.1601\left(A/A_p\right)^3 - 2.7083\left(A/A_p\right)^2 + 16.414\left(A/A_p\right) - 14.044 \tag{55}$$

Therefore the value of $\Delta\alpha$ is

$$\Delta\alpha = \alpha_{us} \tag{56}$$

Equation (45) becomes

$$\frac{P_e}{P_0} = (1 + [\alpha_{ss} + \alpha_{us}]) \frac{A_p}{A} \frac{P_{tp}}{P_0} \sqrt{\frac{T_e}{T_{tp}}} \left(\frac{2}{1+\gamma} \right)^{\frac{\gamma+1}{2(\gamma-1)}} \tag{57}$$

From this equation, the total pressure ratio P_{te}/P_0 can then be determined as [2]

$$\frac{P_{te}}{P_0} = \frac{P_e}{P_0} \left(\frac{1+\gamma}{2} \right)^{\frac{\gamma}{(\gamma-1)}} \tag{58}$$

The ejector pressure ratio is then found to be

$$\pi_{ejec} = \frac{P_{te}}{P_0} \frac{P_0}{P_{ts}} \tag{59}$$

Reference [4] illustrates the engine performance equations in a form that can be easily followed. A detailed step-by-step derivation of these equations is shown in Appendix A. The engine performance equations for specific thrust, specific fuel consumption and thermal and propulsive efficiencies are

$$\frac{F}{\dot{m}_0} = a_0 \left[(1+f) \frac{V_9}{a_0} - M_0 + (1+f) \frac{T_9/T_0}{V_9/a_0} \frac{1 - P_0/P_9}{\gamma} \right] \tag{60}$$

$$S = \frac{f}{F/\dot{m}_0} \tag{61}$$

$$\eta_T = \frac{a_0{}^2 [(1+f)(V_9/a_0)^2 - M_0^2]}{2gfh_{PR}} \tag{62}$$

$$\eta_P = \frac{2gV_0(F/\dot{m}_0)}{a_0{}^2 [(1+f)(V_9/a_0)^2 - M_0^2]} \tag{63}$$

CHAPTER 3

RESULTS

3.1 Introduction

Engine parametric studies are performed based on the equations developed in Chapter 2 and summarized in this chapter. Parameters such as detonation tube length, ejector area ratio, and detonation tube filling time were analyzed with respect to the engine efficiencies, thrust densities and ejector pressure ratios. Three fuels used by the PDE were included. Due to the large number of calculations involved in this analysis, an Excel™ spreadsheet was developed. The spreadsheet contains all the analytical equations derived in the previous chapter and it can be further extended for future analysis for different engine parameters. Several case studies are discussed in this chapter, where at the end, the trend of each engine parameter on the PDE and overall engine performance is discussed.

3.2 Discussion of the spreadsheet used

The Excel™ tool has three sections for data entry and three sections of data output. The first data entry section, shown in Figure 3.1, relates to the detonation tube values, where most of the numbers were obtained using the CEA code [13]. Data in this section focuses mostly on the CJ wave's thermodynamic properties. The data entry is either manual which includes the dark-blue and the white colored boxes in the Excel™ sheet shown in Figure 3.1 or only key values can be entered which are the dark-blue-

colored boxes in Figure 3.1. The rest of the entry values are calculated automatically. For instance, the user can obtain the sonic speed of the undisturbed detonable mixture and the speed of the CJ wave from the CEA code, and the value of the CJ Mach number is calculated by the developed tool, or, the three values can be entered manually from the CEA code. There is a segment at each section where a range of data is entered, and therefore, a range of data output is produced. This will help to produce analysis graphs.

	A	B	C	D	E	F	G	H	I	J	K
1	**DETONATION TUBE INPUT**										
2	**INPUT**	**Symbol**	**Units**	**Value >>**	**Range of Values**						
3	Sonic speed of gas at the undisturbed detonable mixture	a1	m/s	384	384	384	384	384	384	384	384
4	Mass density of the undisturbed detonable mixture	ρ1		0.949	0.949	0.949	0.949	0.949	0.949	0.949	0.949
5	Thermodynamic pressure of the undisturbed detonable mixture gas	p1	kg/m^3	100000	100000	100000	100000	100000	100000	100000	100000
6	Mach number of Chapman-Jouguet detonation wave	M.cj		6.091	6.091	6.091	6.091	6.091	6.091	6.091	6.091
7	Chapman-Jouguet detonation speed of detonable mix	D.cj	m/s	2339	2339	2339	2339	2339	2339	2339	2339
8	Heat released in chemical reaction per unit mass	q	Joule/Kg	9878875.045	9878875	9878875	9878875.045	9878875.045	9878875	9878875.045	9878875.05
9											
10	specific-heat ratio of the undisturbed detonable mixture	γ.1		1.4	1.4	1.4	1.4	1.4	1.4	1.4	1.4
11	specific-heat ratio of the CJ surface of detonation wave	γ.2		1.13	1.13	1.13	1.13	1.13	1.13	1.13	1.13
12	time relative to instant of ignition	t (changing))	sec	0.001	0.001	0.001	0.001	0.001	0.001	0.001	0.001
13	x coordinate along axis of PDE	x (changing)	m	1	1	1	1	1	1	1	1
14	Length of PDE	L (m)	m	1.5	1.5	1.5	1.5	1.5	1.5	1.5	1.5
15	duration of filling phase	taw f (changin	sec	0.002	0.002	0.0022	0.0024	0.0026	0.0028	0.003	0.0032
16	purge time	t purge	sec	0.002	0.002	0.0022	0.0024	0.0026	0.0028	0.003	0.0032

Figure 3.1 Section one - detonation tube data entry.

The output part of the first section, shown in Figure 3.2, contains the derived equations of the CJ wave properties and time, full cycle time, thrust and impulse density values.

The second section of the Excel™ sheet is shown in Figure 3.3. This section focuses on the ejector and mixing area region, where different values such as the ejector area ratio and the primary and secondary mass flow values are input. The output from this section shown in Figure 3.4 is the primary and secondary Mach numbers just before mixing, the bypass ratio value, and the ejector pressure and temperature ratios.

The final section relates to the overall engine performance, where different values of the engine are asked such as: inlet Mach number, temperatures, specific heats and some theoretically assumed pressure ratios. The input part of this section is shown in Figure 3.5.

56	Detonation tube output									
57	OUTPUT									
58	At the Chapman-Jouguet surface:									
59	Mass density	row 2	kg/m^3	1.790	1.790	1.790	1.790	1.790	1.790	1.790
60	Thermodynamic pressure	p2	Pa	2438632.891	2438632.9	2438632.9	2438632.891	2438632.891	2438632.9	2438632.891
61	Flow velocity of CJ det. Wave surface	u2	m/sec	1098.122	1098.122	1098.122	1098.122	1098.122	1098.122	1098.122
62	speed of detonable mix	D2=Dcj	m/sec	2339	2339	2339	2339	2339	2339	2339
63	Sonic speed of gas	a2	m/sec	1240.878	1240.878	1240.878	1240.878	1240.878	1240.878	1240.878
64										
65	the position of the CJ surface	x2(changing)	m	2.339	2.339	2.339	2.339	2.339	2.339	2.339
66										
67	Von Nuemann Spike condition:									
68	Mass density of Von Neumann spike	row N	kg/m^3	5.697	5.697	5.697	5.697	5.697	5.697	5.697
69	Thermodynamic pressure of Von Neumann spike	pN	Pa	4328573.382	4328573.4	4328573.4	4328573.382	4328573.382	4328573.4	4328573.382
70										
71	the state of the flow inside the rarefaction wave									
72		row	kg/m^3	0.627	0.627	0.627	0.627	0.627	0.627	0.627
73		p	Pa	746066.9632	746066.96	746066.96	746066.9632	746066.9632	746066.96	746066.9632
74		u	m/sec	-159.155	-159.155	-159.155	-159.155	-159.155	-159.155	-159.155
75		a	m/sec	2257.277	2257.277	2257.277	2257.277	2257.277	2257.277	2257.277
76										
77	gas condition at the rare boundary of rarefaction following the det.									
78	the position of the rare boundary	x3	m	1.170	1.170	1.170	1.170	1.170	1.170	1.170
79	the propagation velocity	D3=a3	m/sec	1169.5	1169.5	1169.5	1169.5	1169.5	1169.5	1169.5
80	Mass density	row3	kg/m^3	0.719	0.719	0.719	0.719	0.719	0.719	0.719
81	Thermodynamic pressure	P3	Pa	870683.900	870683.900	870683.900	870683.900	870683.900	870683.900	870683.900
82										
83	time when the det. Exit the open end	t1	sec	0.0013	0.0013	0.0013	0.0013	0.0013	0.0013	0.0013
84	time for wave travel from open to close end	t2	sec	0.0026	0.0026	0.0026	0.0026	0.0026	0.0026	0.0026
85			sec	0.0026	0.0026	0.0026	0.0026	0.0026	0.0026	0.0026
86										
87	External gas condition									
88	Mass density	row ext	kg/m^3	0.273	0.273	0.273	0.273	0.273	0.273	0.273
89	Thermodynamic pressure	p ext	Pa	291338.65	291338.65	291338.65	291338.65	291338.65	291338.65	291338.65
90	flow velocity	u ext	m/sec	1098.12	1098.12	1098.12	1098.12	1098.12	1098.12	1098.12
91	the mass exhaust rate per unit area	row ext * u ext	kg/sec	299.80	299.80	299.80	299.80	299.80	299.80	299.80
92		V		1098.12	1098.12	1098.12	1098.12	1098.12	1098.12	1098.12
93		M		2.86	2.86	2.86	2.86	2.86	2.86	2.86
94										
95	the period of the exhaust phase	t3-t1	sec	0.0036	0.0036	0.0036	0.0036	0.0036	0.0036	0.0036
96	time for the gas to be exhausted	t3	sec	0.0049	0.0049	0.0049	0.0049	0.0049	0.0049	0.0049
97										
98	Pressure acting on the thrust wall	Pw	Pa	1458961.33	1458961.3	1458961.3	1458961.33	1458961.33	1458961.3	1458961.33
99		Pw/P1		14.59	14.59	14.59	14.59	14.59	14.59	14.59
100	The period of the cycle	Tcyc	sec	0.01	0.01	0.01	0.01	0.01	0.01	0.01
101	frequency of cycle	fcyc	1/sec	112.59	112.59	107.74	103.29	99.19	95.40	91.90
102										
103	Impulse density acting on thrust wall per one cycle operation	I cyc		3241.98	3241.98	3241.98	3241.98	3241.98	3241.98	3241.98
104	the average thrust density	Pave	pa	365014.94	365014.94	349284.56	334853.97	321568.46	309296.94	297927.59

Figure 3.2 Section one - detonation tube data output.

18	EJECTOR TUBE INPUT									
19	Primary Flow:									
20	Stagnation pressure		Pa	365014.940	365014.940	349284.557	334853.967	321568.459	309296.940	297927.591	287364.451
21	Primary flow pressure ratio: Ptp/Po			3.604	3.604	3.449	3.306	3.175	3.054	2.942	2.837
22	Total Temperature		K	4674.867	4674.867	4473.403	4288.586	4118.434	3961.269	3815.657	3680.372
23			K	4674.867	4674.867	4473.403	4288.586	4118.434	3961.269	3815.657	3680.372
24	Temperature ratio Ttp/To			16.232	16.232	15.533	14.891	14.300	13.754	13.249	12.779
25	Area ratio			1.7	1.7	1.7	1.7	1.7	1.7	1.7	1.7
26	gamma			1.13	1.13	1.13	1.13	1.13	1.13	1.13	1.13
27										
28	Secondary flow:									
29	Mo			2	2	2	2	2	2	2	2
30	Pressure ratio : Pts/Po			7.238	7.238	7.238	7.238	7.238	7.238	7.238	7.238
31	Temperature ratio : Tts/To			1.8	1.8	1.8	1.8	1.8	1.8	1.8	1.8
32	gamma			1.4	1.4	1.4	1.4	1.4	1.4	1.4	1.4
33	Pi/Po			0.912	0.912	0.912	0.912	0.912	0.912	0.912	0.912

Figure 3.3 Section two - ejector and mixing area region input.

108	Ejector Tube output									
109	inlet plane flow properties:									
110	inlet primary mach number	Mpi		1.62	1.62	1.59	1.57	1.54	1.51	1.49
111	area ratio of inlet primary flow and primary flow throat area	Api/Ap*		1.34	1.34	1.31	1.28	1.26	1.23	1.21
112		Api/A		0.79	0.79	0.77	0.75	0.74	0.72	0.71
113		Asi/A		0.21	0.21	0.23	0.25	0.26	0.28	0.29
114		Msi		2.03	2.03	2.03	2.03	2.03	2.03	2.03
115	bypass ratio	alfa steady		1.04	1.04	1.16	1.27	1.38	1.49	1.59
116		alfa unsteady		6.82	6.82	6.82	6.82	6.82	6.82	6.82
117		Alfa		7.86	7.86	7.98	8.09	8.20	8.31	8.41
118	exit plane properties:									
119	exit temperature ratio	Te/Ttp		0.20	0.20	0.20	0.20	0.21	0.21	0.21
120	Exit presure ratio	Pe/Pts		4.99	4.99	4.88	4.77	4.67	4.58	4.49
121	Total ejector pressure ratio	Pte/Pts		8.63	8.63	8.43	8.25	8.08	7.92	7.77
122		Te		927.19	927.19	900.34	876.10	854.13	834.14	815.88

Figure 3.4 Section two - ejector and mixing area region output.

35	ENGINE PERFORMANCE INPUT									
36	**engine performance**									
37	Mach number toward the engine	Mo		2	2	2	2	2	2	2
38	Total temperature entering the engine	To [Te]	K	216	216	216	216	216	216	216
39	Specific Heat Ratio of the mixed flow	gamma ejec.		1.3	1.3	1.3	1.3	1.3	1.3	1.3
40		Cp ejec	KJ/(g.K)	1.004	1.004	1.004	1.004	1.004	1.004	1.004
41	Specific Heat Ratio of the mixed flow	gamma		1.3	1.3	1.3	1.3	1.3	1.3	1.3
42		Cp	kj/(kg.K)	1.004	1.004	1.004	1.004	1.004	1.004	1.004
43		Hpr	kj/kg	42800	42800	42800	42800	42800	42800	42800
44		pi d max		0.9	0.9	0.9	0.9	0.9	0.9	0.9
45		pi b		0.95	0.95	0.95	0.95	0.95	0.95	0.95
46		pi n		0.95	0.95	0.95	0.95	0.95	0.95	0.95
47		e ejec		1	1	1	1	1	1	1
48				1	1	1	1	1	1	1
49		eff b		0.98	0.98	0.98	0.98	0.98	0.98	0.98
50		eff m		1	1	1	1	1	1	1
51		P0/P9		0.7	0.7	0.7	0.7	0.7	0.7	0.7
52	the temperature at the end of the after burner	Tt4	K	1524.898	1524.898	1472.729	1425.758	1383.273	1344.681	1309.490
53		pi ejec		8.634	8.634	8.434	8.249	8.077	7.917	7.768
54	Universal gas constant	R		0.232	0.232	0.232	0.232	0.232	0.232	0.232

Figure 3.5 Section three - whole engine performance input.

The output of this section is shown in Figure 3.6. It shows the result of the engine performance values such as: thermal and propulsive efficiencies, engine specific thrust, and specific fuel consumption.

132	Engine Performance output									
133										
134	Universal Gas Constant	R	kJ/(Kg.K)	0.2317	0.2317	0.2317	0.2317	0.2317	0.2317	0.2317
135		R	kJ/(Kg.K)	0.2317	0.2317	0.2317	0.2317	0.2317	0.2317	0.2317
136	Sonic speed of gas entering the burner	ao	m/sec	255.07	255.07	255.07	255.07	255.07	255.07	255.07
137		Vo	m/sec	510.13	510.13	510.13	510.13	510.13	510.13	510.13
138	Total to static temperature ratio of the free stream	taw r		1.6	1.6	1.6	1.6	1.6	1.6	1.6
139	total to static pressure ratio of the free stream	pi r		7.67	7.67	7.67	7.67	7.67	7.67	7.67
140		eff r		0.93	0.93	0.93	0.93	0.93	0.93	0.93
141	defuser pressure	pi d		0.83	0.83	0.83	0.83	0.83	0.83	0.83
142	Burner exit enthalpy to the ambient enthalpy	taw lamda		7.06	7.06	6.82	6.60	6.40	6.23	6.06
143	N/A	taw ejec		1.64	1.64	1.64	1.63	1.62	1.61	1.60
144	N/A	eff ejec		1	1	1	1	1	1	1
145	Fuel to air ratio	f		0.0238	0.0238	0.0225	0.0214	0.0204	0.0195	0.0187
149	Nozzle pressure ratio	Pt9/p9		34.81	34.81	34.00	33.25	32.56	31.92	31.32
150	Mach number at nozzle	M9		2.91	2.91	2.89	2.88	2.87	2.86	2.84
151	Temperature ratio at nozzle	T9/To		3.11	3.11	3.02	2.94	2.87	2.80	2.74
152	vehicle mach number	V9/a0		5.13	5.13	5.03	4.94	4.86	4.78	4.71
153	specific thrust	F/Mo	N/(kg/sec)	866.07	866.07	838.12	812.61	789.23	767.73	747.89
154	Specific fuel consumption	S	g.sec/N	2.74385E-05	2.744E-05	2.686E-05	2.633E-05	2.58342E-05	2.537E-05	2.49405E-05
155	Thermal efficiency	eff T		0.734	0.734	0.739	0.743	0.748	0.752	0.757
156	Propulsive efficiency	eff P		0.592	0.592	0.601	0.609	0.617	0.624	0.631
157	overall efficiency	eff O		0.434	0.434	0.444	0.453	0.461	0.470	0.478

Figure 3.6 Section three - whole engine performance output.

This tool can be further improved. Some suggested improvements are:

- Embed the spreadsheet with an equation editor where it will be easy to see the equations used for each data output.

- Locking some of the cells so that no entries are made on them, and therefore, no changes are made on programmed equations
- Having a similar sheet that uses English rather than SI units.

3.3 Discussion of Selected Case Studies

3.3.1 Case study 1

This case examines the effect of changing the detonation tube filling time t_{fill} on the PDE thrust density P_{ave}, the ejector pressure ratio π_{ejec}, and thermal and propulsive efficiencies. For this case the incoming flow Mach number is 2, the inlet temperature is 216.7 K. The filling time of the detonation tube t_{fill} is varied from 1 to 2.6 ms for a tube length of 0.5 m, from 1.5 to 3.1 ms for tube length of 1 m, and finally from 2 to 3.6 ms for a tube length of 1.5 m. The ejector area ratio is $A/A_p = 1.7$ and the fuel used for this case is hydrogen, with oxygen for oxidizer.

Figure 3.7 shows that the average thrust density P_{ave} changes clearly with the change of the filling time t_{fill}. In addition, for longer tube lengths, the amount of thrust produced from the detonation tube is larger. The gain in the amount of thrust for this period of filling time is higher than when the detonation tube is shorter.

The variation in filling time, in Figure 3.8, has an almost similar effect on the ejector pressure ratio as it has on the thrust density. At longer detonation tube and short filling times, the pressure increase across the ejector is much higher. The amount of gain for the shorter tube, however, is higher for the same period of filling time. This

can be seen from the slope of the graph on Figure 3.8 for detonation tube length of 0.5 m.

The thermal efficiency in Figure 3.9 has a proportional relation with the increase of the filling time t_{fill}. A shorter tube length produces a higher value of thermal efficiency. As the length of the tube gets longer this proportional relation becomes linear and the increase in thermal efficiency becomes less. The propulsive efficiency η_P, shown in Figure 3.10, behaves similarly to the thermal efficiency. As the tube length gets shorter and the filling time period gets longer, the propulsive efficiency increases.

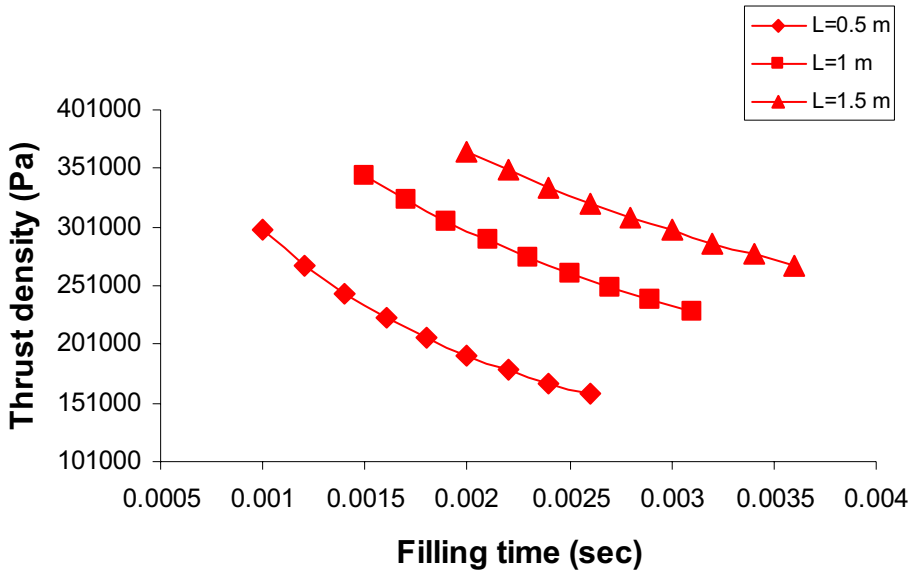

Figure 3.7 The effect of detonation tube filling time on detonation thrust density.

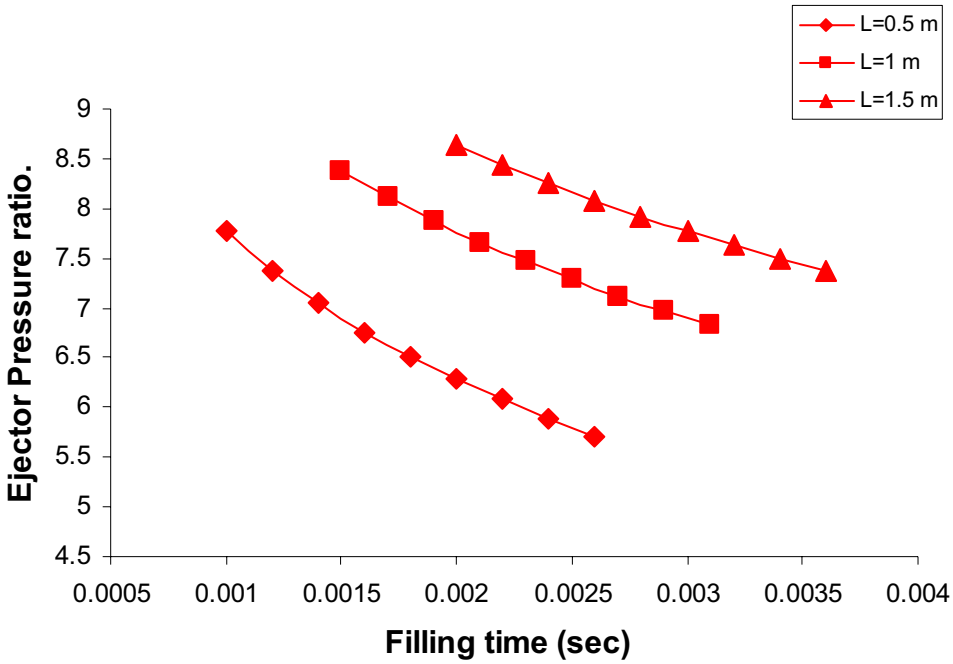

Figure 3.8 The effect of detonation tube filling time on pressure ratio across the ejector.

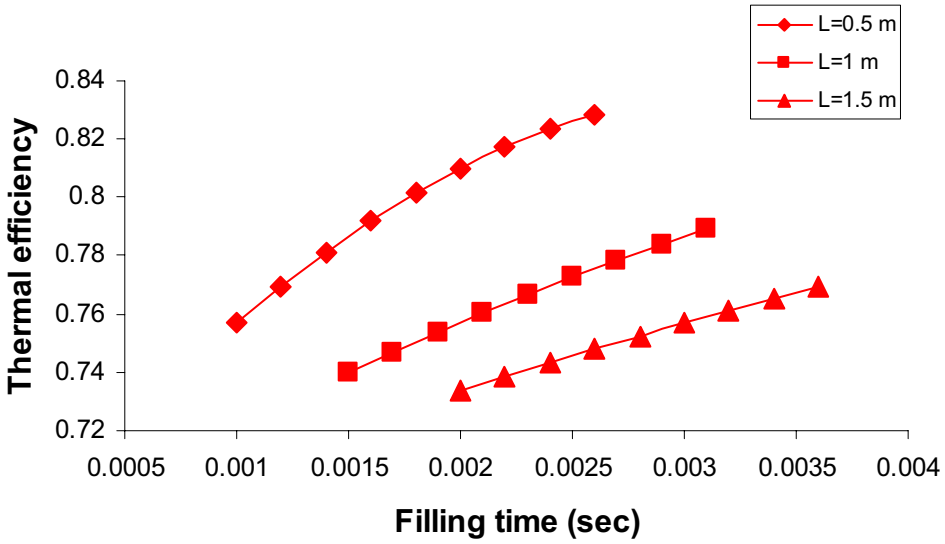

Figure 3.9 The effect of detonation tube filling time on engine thermal efficiency.

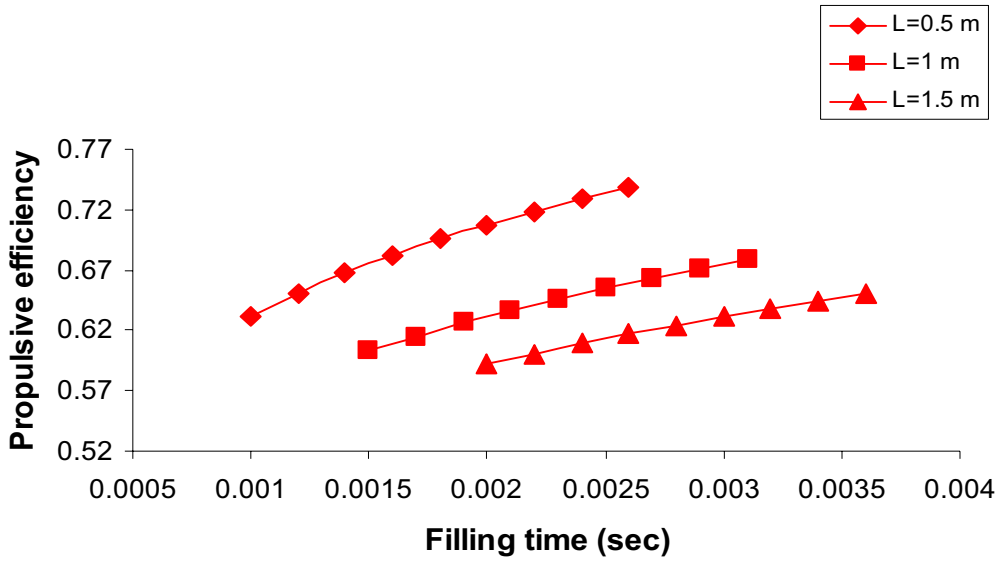

Figure 3.10 The effect of detonation tube filling time on engine propulsive efficiency.

3.3.2 Case study 2

In this case study, the effect of changing the ejector area ratio on the engine performance is analyzed. The filling time in this case is chosen to be the optimum from case study 1. Where at tube length of 0.5 m the filling time is set to be equal to 1.4 ms, at tube length of 1 m the filling time is 2 ms and finally at tube length of 1.5 m the filling is 2.5 ms. The ejector area ratio is varied from 1.2 to 9.2, and the engine flight conditions are similar to case study 1.

The engine ejector pressure ratio π_{ejec} almost doubles as the ejector area ratio increases from 1.2 to 2.5. The pressure across the ejector decreases as the area ratio increases from 2.5 till 8, then it starts to increase for area ratios greater than 8. Longer tube lengths seem to produce a higher pressure increase across the ejector. The differences in tube lengths have a minimal effect as the area ratio becomes smaller.

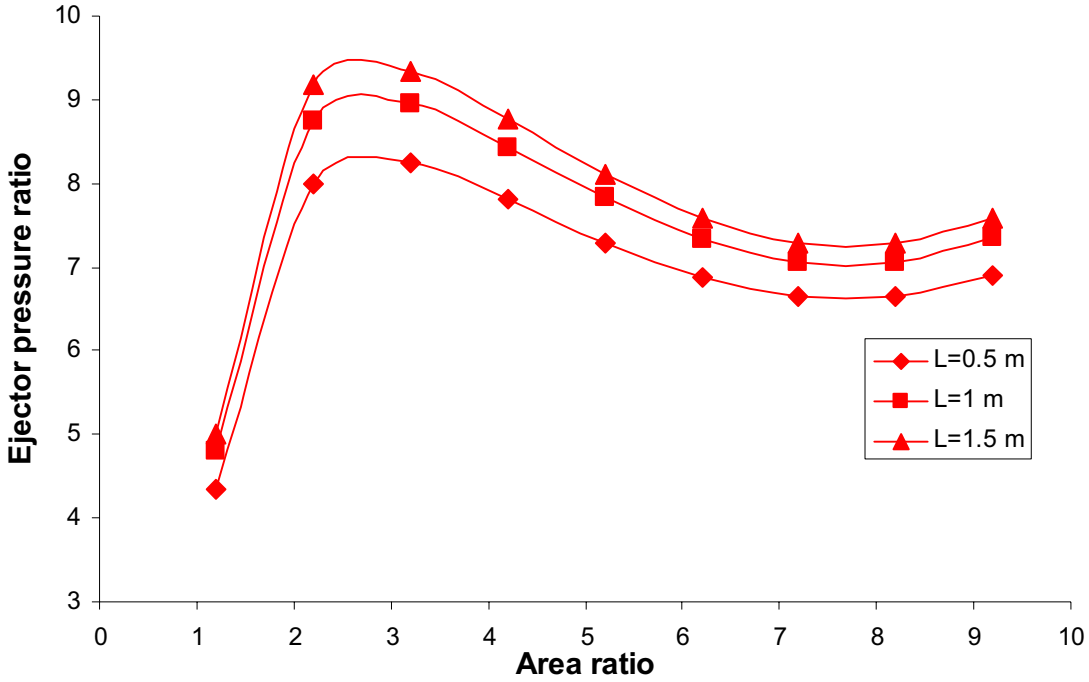

Figure 3.11 The effect of the ejector area ratio on ejector pressure ratio.

The propulsive efficiency increases significantly with the increase of the area ratio. Most of the increase in the efficiency occurs between an area ratio of 1.2 and 2.2. The effect of the tube length becomes clear as the area ratios become smaller. Shorter tube lengths give a higher value of propulsive efficiency. The thermal efficiency in Figure 3.13 increases as the area ratio of the ejector gets higher. The detonation tube length has almost no effect on the engine thermal efficiency as the area ratio becomes smaller. Shorter tube lengths produce higher value of engine thermal efficiencies.

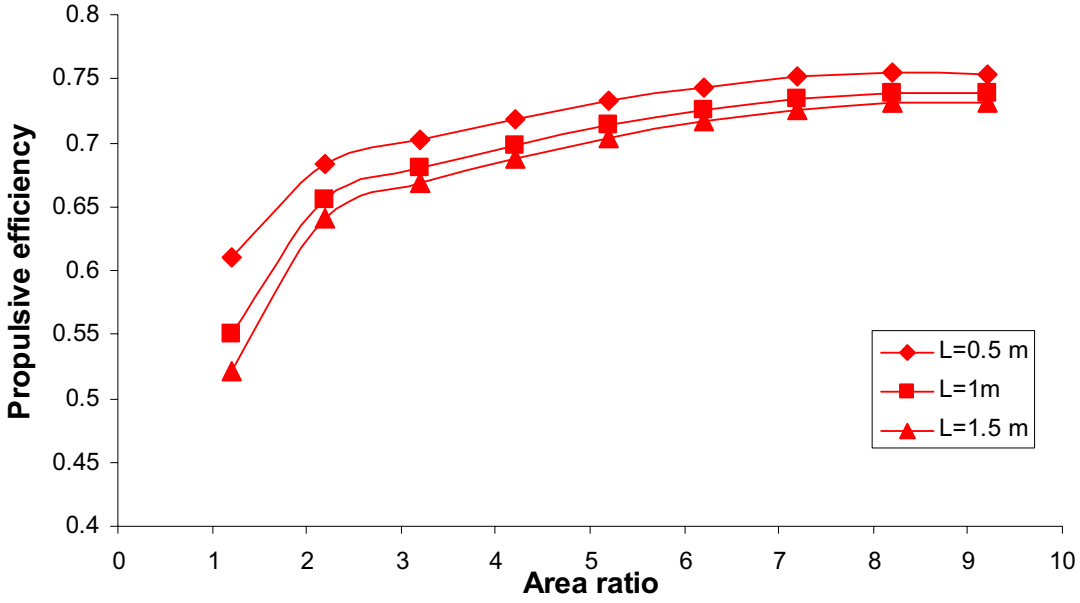

Figure 3.12 The effect of the ejector area ratio change on engine propulsive efficiency.

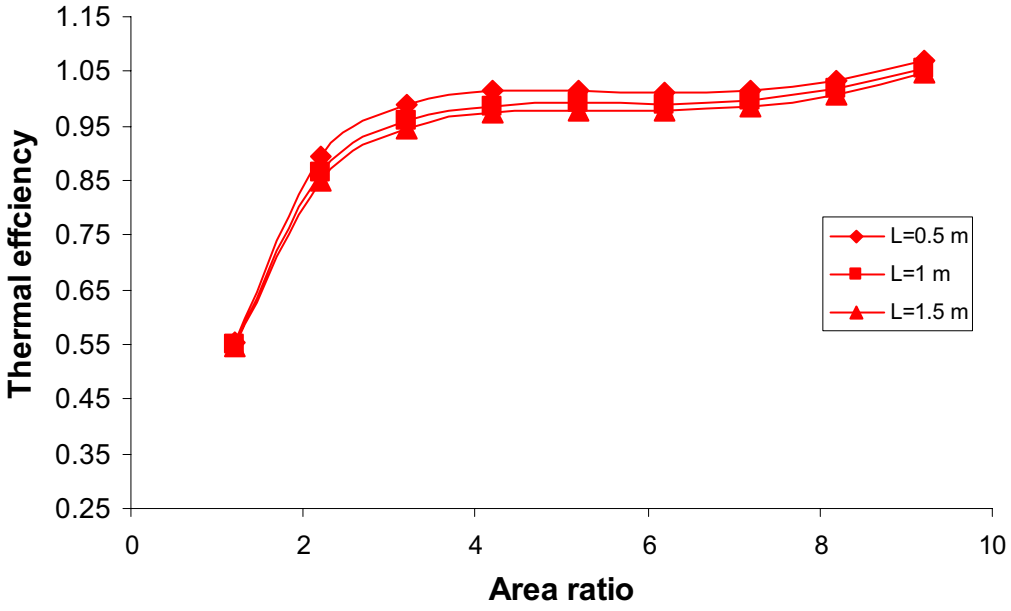

Figure 3.13 The effect of the ejector area ratio change on engine thermal efficiency.

3.3.3 Case study 3

In this case study, the effect of unsteadiness in the primary flow of the PDE is analyzed. A comparison study is made between a steady and unsteady ejectors that shows the behavior of the engine performance when an unsteadiness in the primary flow is introduced. The tube length is set to 1.5 m, the filling time is set to 2 ms and the ejector area ratio is varied from 1.2 to 9.2.

The engine ejector pressure ratio π_{ejec} almost triples as the unsteadiness into the primary flow is introduced, see Figure 3. 14. The rapid increase in π_{ejec} for both steady and unsteady flows occurs when the area ratio changes from 1.2 to around 2.5. The increase in π_{ejec} is almost negligible for area ratios greater than 2.5 for the steady flow. The behavior of the unsteady flow is analyzed in the previous case study (case study 2). The thermal efficiency increases clearly for the unsteady ejector. For smaller area ratios the difference in thermal efficiency is small, as the ratio gets larger the different in thermal efficiency between the steady and the unsteady flow becomes larger especially between an area ratio of 2 and 4.

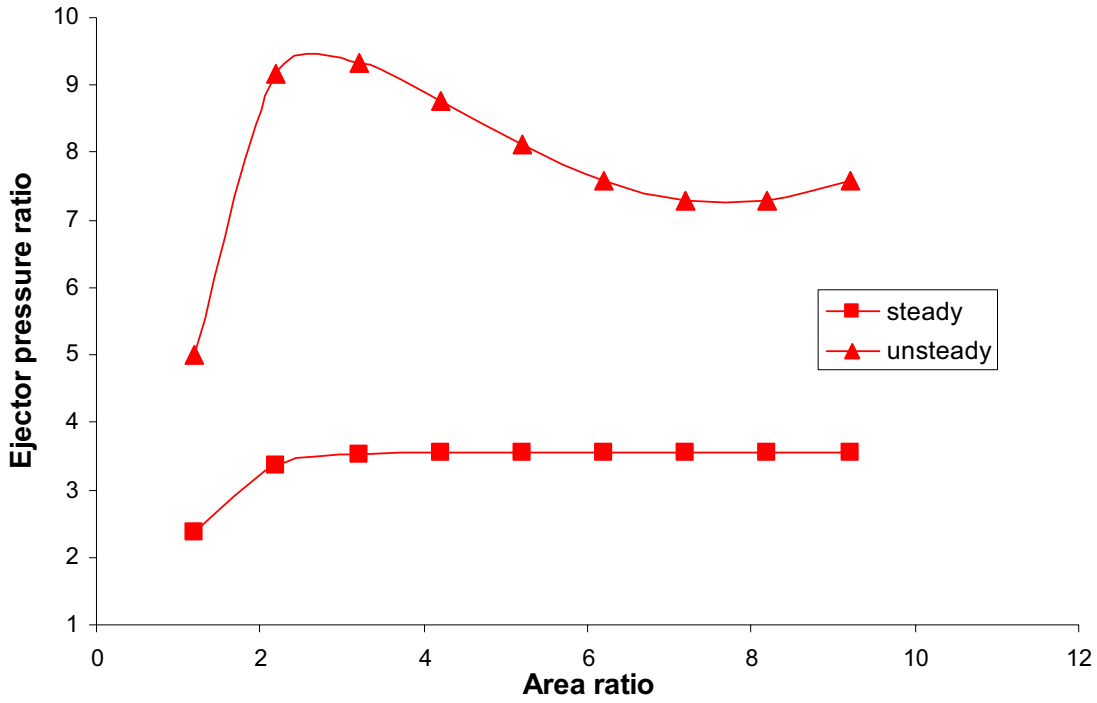

Figure 3.14 The effect of the ejector area ratio on ejector pressure ratio.

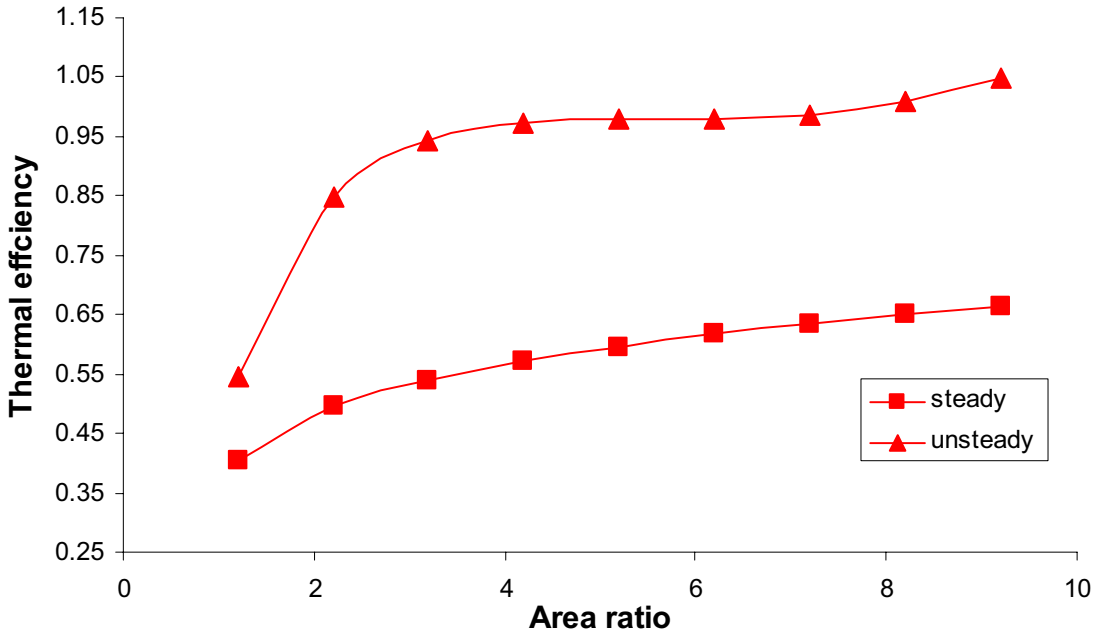

Figure 3.15 The effect of the ejector area ratio change on engine propulsive efficiency.

At small area ratios, the propulsive efficiency for the unsteady ejector, in Figure 3.16, is higher than the steady one. As the area ratio becomes greater than 3 the steady ejector starts to produce higher efficiency. The area ratio increase for the ejector has a proportional effect on engine performance for both steady and unsteady primary flows.

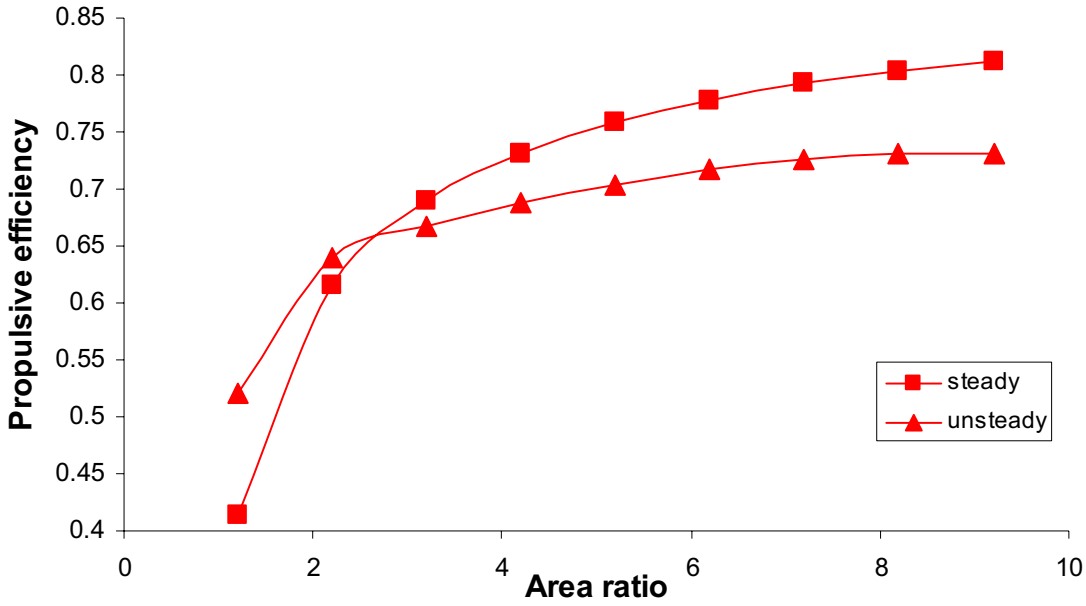

Figure 3.16 The effect of the ejector area ratio change on engine thermal efficiency.

Cases 4 to 6 focus on the behavior of using three different types of propellant mixtures for the PDE on the engine performance. For this analysis, the CEA code was used for similar flight conditions as in cases 1 and 2. The fuels that are used are hydrogen, methane and propane. The reactant for the three fuels is air.

3.3.4 Case study 4

Case 4 is a study on the effect of changing the detonation tube length on the engine performance when three different propellants are used on the PDE. In this case

the detonation tube length is changed from 0.5 to 2.1 m while the ejector area ratio is set to 1.7. The detonation filling time is set to an optimum of 1 ms for the whole range of detonation tube lengths.

The tube length change has a big influence on the thrust produced from the detonation tube. As shown in Figure 3.17, there is a large gain in the thrust as the tube length gets longer. At a shorter length, that is 0.5 m, hydrogen and propane give almost the same value of thrust from the PDE. As the tube length gets longer, the increase in thrust from hydrogen is much larger of that from propane. Methane fuel produces the lowest amount of thrust with similar relation of increment as the other two fuels.

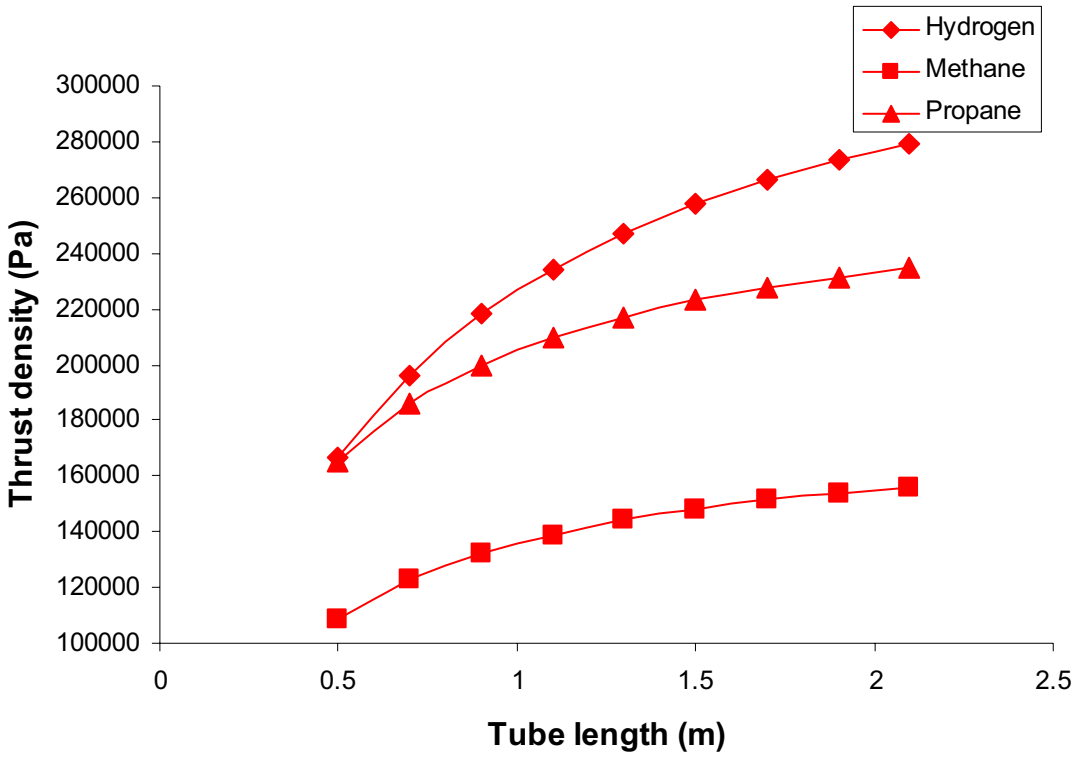

Figure 3.17 The effect of detonation tube length on tube thrust density at different types of fuel.

The pressure increment across the ejector is much higher when propane fuel is used. Methane produces the lowest amount of pressure increment. From Figure 3.18, the three fuels increase the amount of pressure ratio across the ejector as the detonation tube length is increased. However, when methane is used there is a rapid increase in the pressure ratio between tube lengths of 0.5 and 0.8 m.

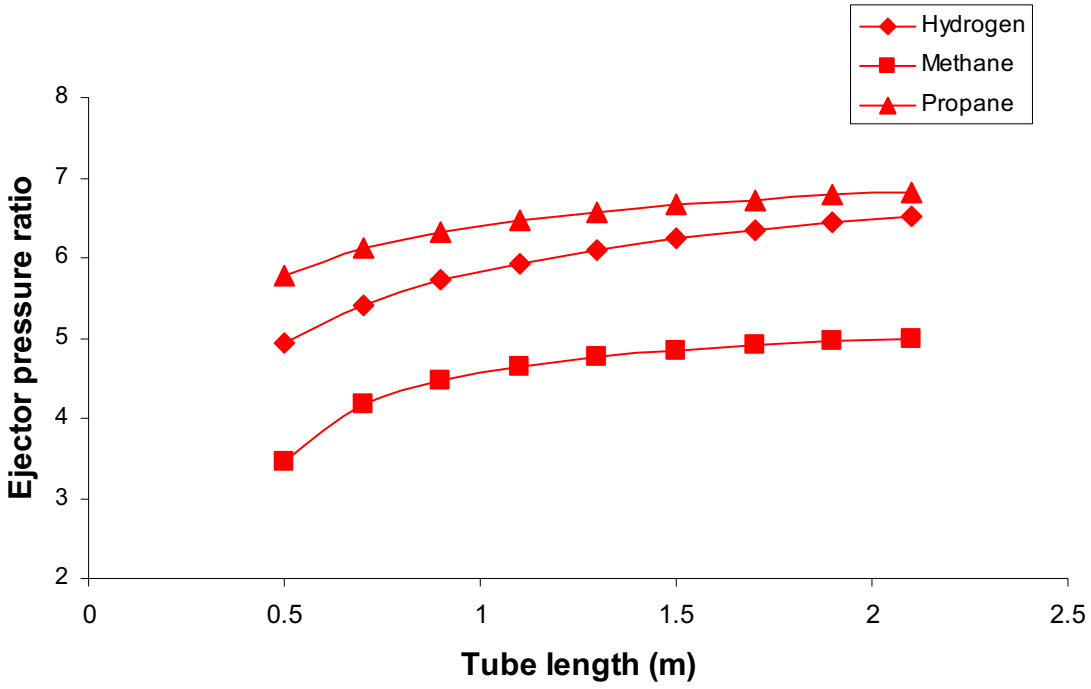

Figure 3.18 The effect of detonation tube length change on ejector pressure ratio.

The propulsive efficiency has an inverse relation with the detonation tube length for the three fuels used. From Figure 3.19, methane produces the highest amount of propulsion efficiency especially at lower tube lengths. Hydrogen produces the lowest efficiency value.

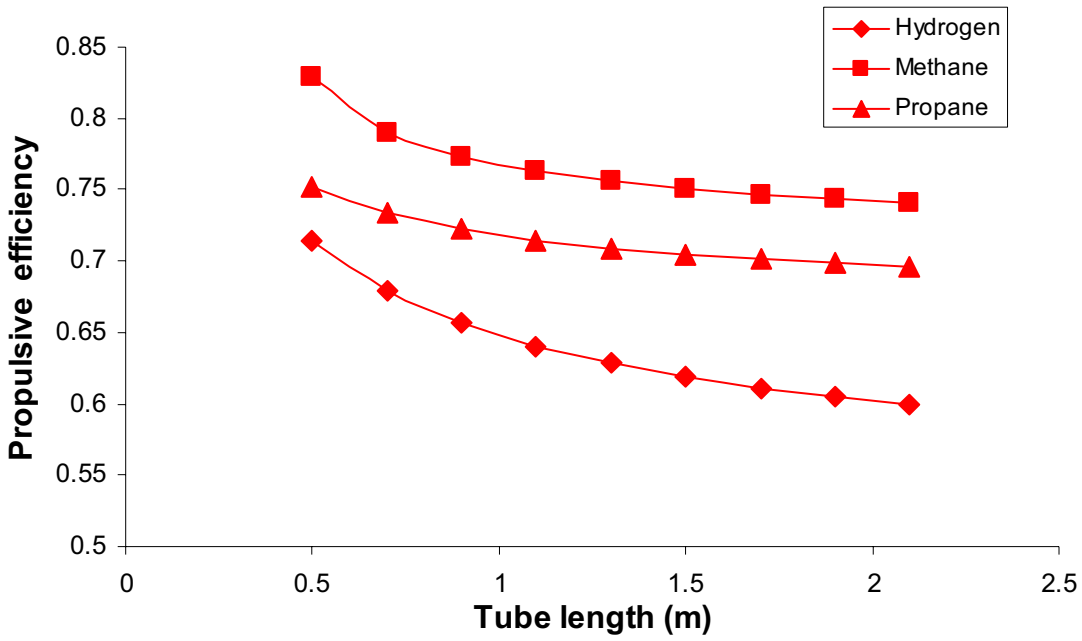

Figure 3.19 The effect of detonation tube length on engine propulsive efficiency.

The change in the tube length, in Figure 3.20, has a different effect on the thermal efficiency. For hydrogen and propane, the thermal efficiency decreases as the tube length increases, where propane produces a higher value of thermal efficiency. Methane behaves in an opposite way; it tends to increase the efficiency as tube length increases and then the efficiency stays constant as the tube length gets longer ($L > 0.8$ m).

3.3.5 Case study 5

This case focuses on the behavior of changing the detonation tube filling time on the engine performance for the three different fuels used. In this case, the detonation tube length is set at 1.5 m, the ejector area ratio is set to 1.7, and the filling time ranges from 1 to 3.8 ms.

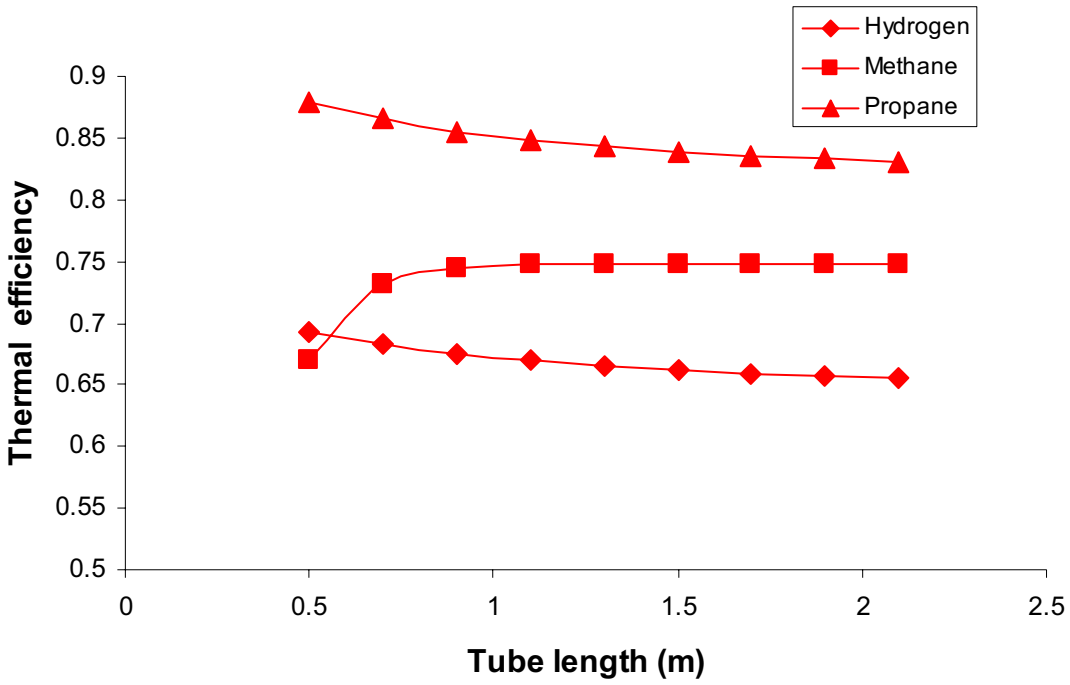

Figure 3.20 The effect of detonation tube length on engine thermal efficiency.

The PDE thrust density is considerably high when hydrogen fuel is used. At higher filling time periods (2.8 ~ 3.4 ms), both hydrogen and propane produces the same amount of thrust, propane tends to produce less thrust compared to hydrogen at shorter filling time. Methane produces the lowest thrust compared to the other two fuels.

The ejector pressure ratio in Figure 3.22 decreases almost linearly with the increase of filling time period when hydrogen and propane fuels are used. Methane suddenly drops the value of the ejector pressure ratio as filling time increases. Propane

produces the highest amount of pressure increment across the ejector, and an optimum value is reached at very small filling time periods.

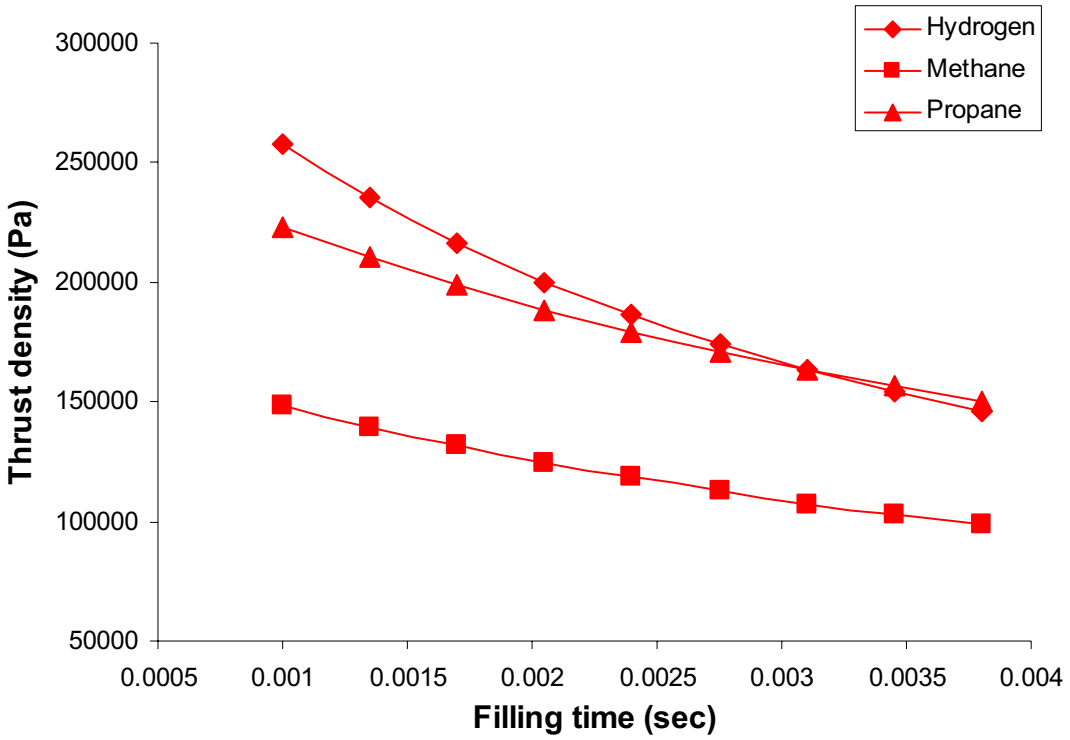

Figure 3.21 The effect of the detonation tube filling time on thrust density.

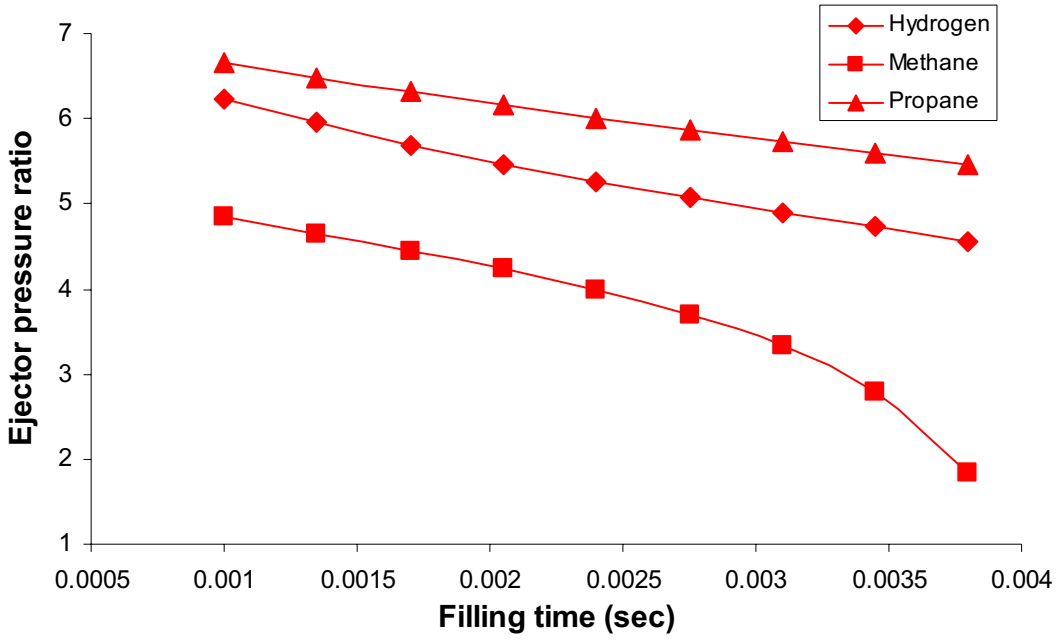

Figure 3.22 The effect of detonation tube filling time on ejector pressure ratio at different types of fuel.

The propulsive efficiency tends to increase with the detonation tube filling time, as seen in Figure 3.23, for the three fuels. Methane produces the best propulsive efficiency in this case, where it approaches 100% at longer periods of filling time. Hydrogen produces the lowest efficiency of the three fuels.

Propane produces the highest thermal efficiency as can be seen in Figure 3.24. Methane produces a higher efficiency compared to hydrogen, but not for filling time periods greater than 2.8 ms where the thermal efficiency drops rapidly. However, both propane and hydrogen linearly increase the thermal efficiency value as the filling time increases.

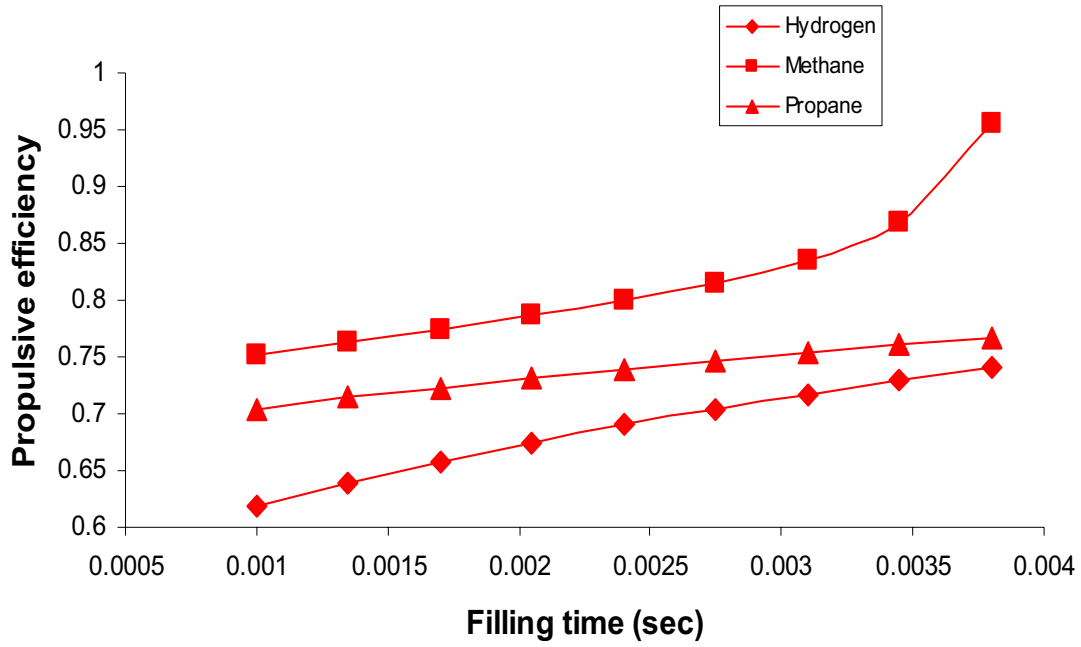

Figure 3.23 The effect of detonation tube filling time on engine propulsive efficiency for different types of fuel.

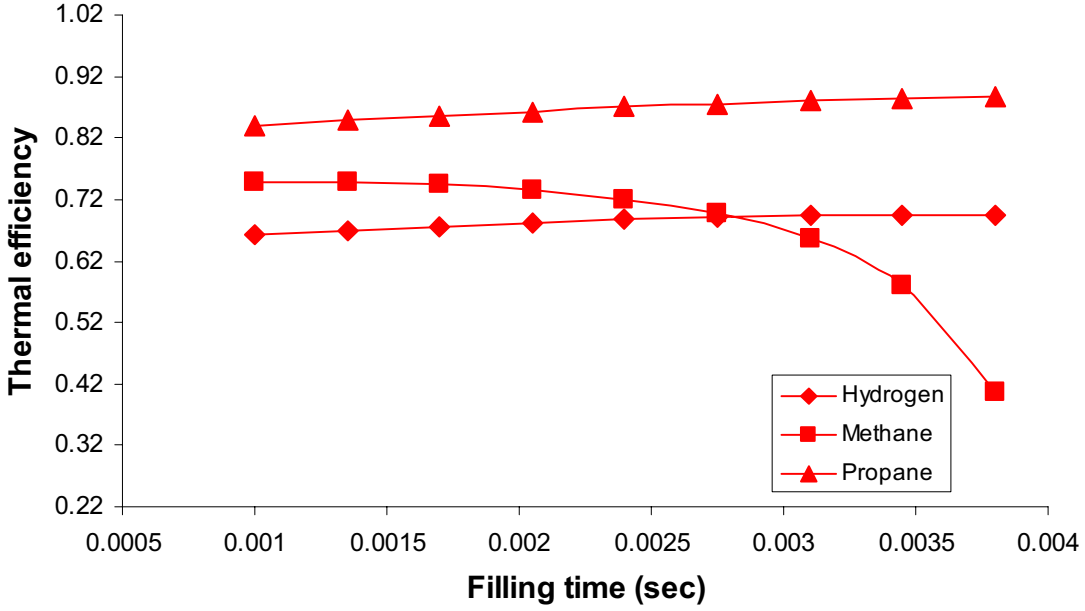

Figure 3.24 The effect of detonation tube filling time on engine thermal efficiency for different types of fuel.

3.3.6 Case study 6

This case focuses on the effect of changing the ejector area ratio on the behavior of the engine performance for the three different types of fuel. In this case, the detonation filling time is set to be 2 ms, the tube length is set to 1.5 meter, and the area ratio range is 1.2 to 9.2. The ejector pressure ratio is seen in Figure 3.25 to increase rapidly for the three fuel types as the ejector area ratio increases from 1.2 to 3. But the pressure ratio decreases for area ratios greater than 3 and less than 8, then it increases again for area ratios greater than 8.

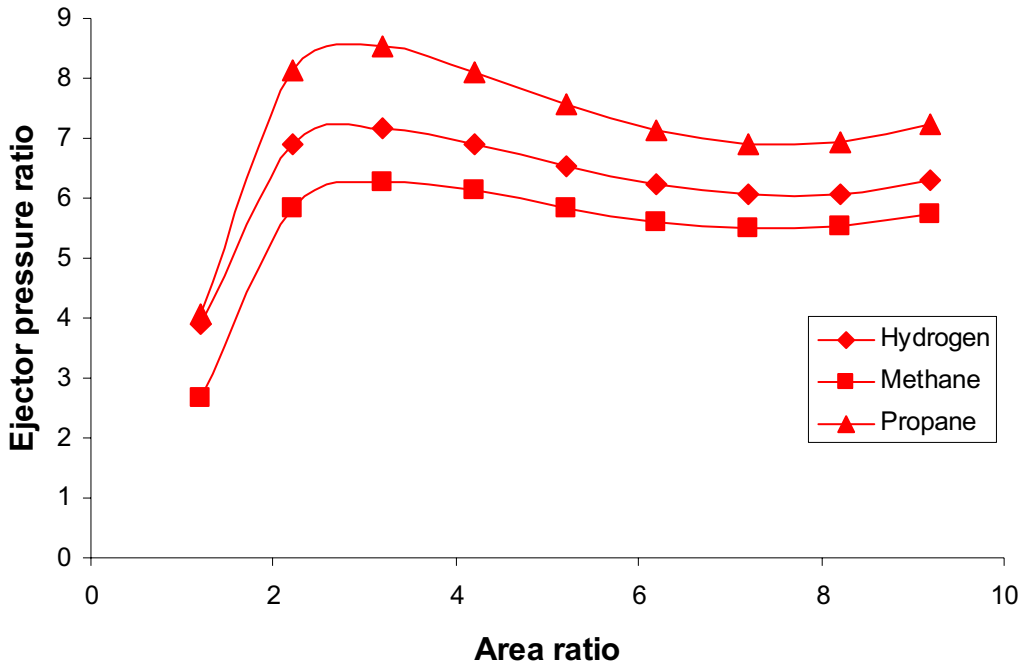

Figure 3.25 The effect of the ejector area ratio on the ejector pressure ratio for different fuel types.

For small area ratios, methane and propane fuels both produces high values of propulsive efficiency. As the area ratio increases to around 2.5, the propulsive

efficiency decreases for the previous two fuels and increases when hydrogen is used. For area ratios greater than 2.5, the propulsive efficiency for the three fuels increases as the ratio of the area increases, with methane and hydrogen producing the highest values.

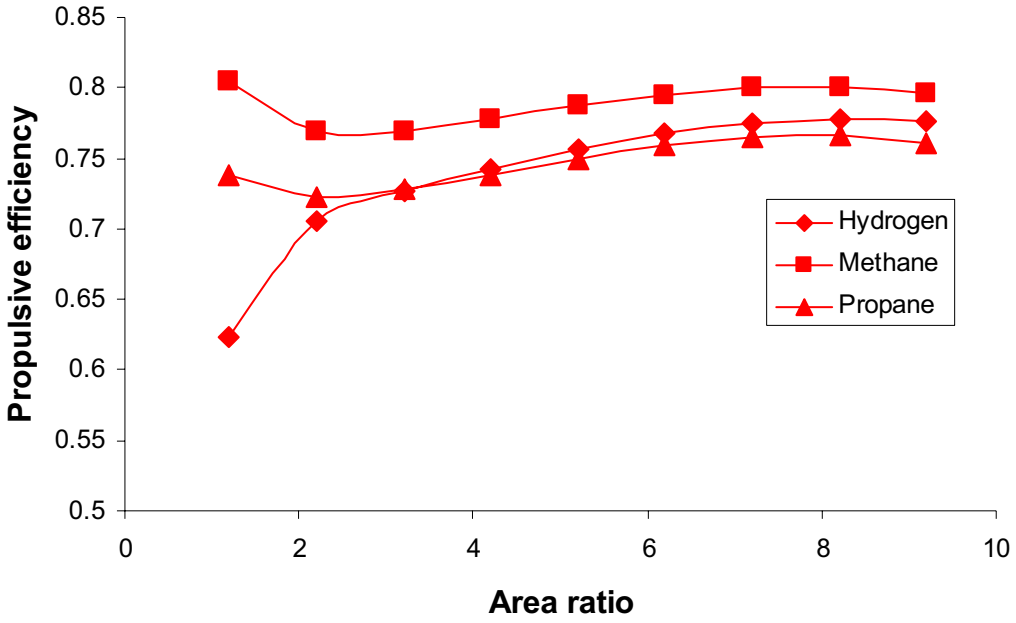

Figure 3.26 The effect of the ejector area ratio change on the engine propulsive efficiency at different fuel types.

The three fuels used for the PDE seem to have a similar effect on the engine thermal efficiency as the ejector area ratio increases. The thermal efficiency rises rapidly for ejector area ratios between 1.2 and 3 for all three fuels considered. At an area ratio greater than 3, the rate of increase decreases. Propane produces the highest value of thermal efficiency. Hydrogen produces the lowest values.

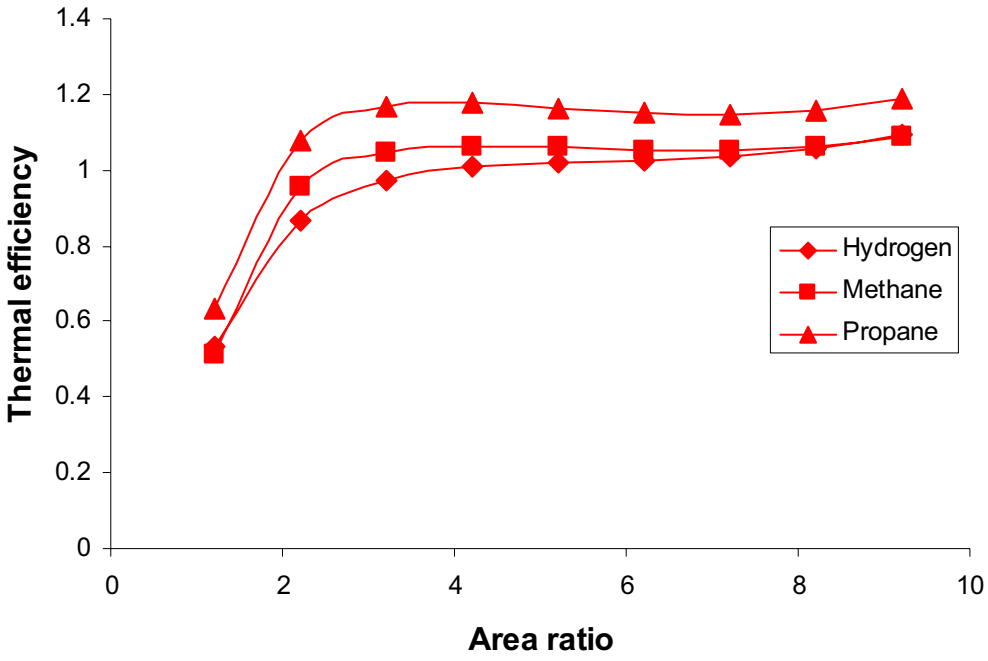

Figure 3.27 The effect of the ejector area ratio on engine thermal efficiency at different fuel type.

CHAPTER 4

CONCLUSIONS

A parametric cycle analysis for an ejector-driven PDE was performed. Different parameters were changed so that an optimum performance can be observed. During this process, an analytical formulation of the gas properties in the detonation tube is achieved. The PDE was modeled as a straight tube, closed at one end and open at the other. The pressure acting on the closed end was calculated using the Hugoniot relation for a Chapman-Jouguet (CJ) detonation wave and flow relations for a self-similar rarefaction wave. The average thrust density p_{ave} is derived. In addition, the pressure ratio across the ejector is also derived.

The results show that a longer detonation tube length, a shorter tube filling time and smaller ejector area ratios yield a higher thrust density and higher pressure across the ejector. The tube length affects the cycle frequency and poses practical problems, for example, in the design of the valve and injection systems. These systems must be capable of fast response times, large mass flow rates and a high degree of controllability. Although reaching a best possible frequency is theoretically possible, any practical design must meet certain cost, weight, volume and power requirements. The unsteadiness in the primary flow is shown to improve the engine performance. The area ratio has a large effect on engine performance.

As an aid to help executing all the analysis calculations, an Excel™ spreadsheet tool is developed for future use. The spreadsheet calculates all the engine performance and gas flow characteristics. Starting from the detonation tube where the PDE cycle time and primary flow thrust is calculated. Then, the mixing flow properties and speed is determined at the end of the ejector. The calculation ends at the afterburner and nozzle region where the overall engine performance and efficiencies are determined.

APPENDIX A

EJECTOR-DRIVEN PDE PERFORMANCE EQUATIONS DERIVATION

Reference [4] illustrates the equations in a form that can be easily followed. Starting by calculating the universal gas constant R

$$R = \frac{\gamma - 1}{\gamma} c_p \tag{A.1}$$

Where the value of the specific heat ratio γ is an input variable and it is around 1.35 for the case of the afterburner [4]. The speed of the stream entering the inlet is the Mach number at the inlet times the sonic speed at that region. The Mach number at the entrance of the inlet is set to 2 for simplicity. The sonic speed a_0 is then found to be equal to

$$a_0 = \sqrt{\gamma R T_0} \tag{A.2}$$

where T_0 is the static temperature at the inlet of the ejector. The total to static temperature and pressure ratios of the free stream entering the ejector τ_r, π_r is defined by

$$\tau_r = \frac{T_{t0}}{T_0} = 1 + \frac{\gamma - 1}{2} M_0^{\,2} \tag{A.3}$$

$$\pi_r = \frac{P_{t0}}{P_0} = \left(1 + \frac{\gamma - 1}{2} M_0^{\,2}\right)^{\gamma/(\gamma-1)} \tag{A.4}$$

The ratio of the after burner exit-enthalpy $c_p T_{t.AB}$ to the inlet entrance-enthalpy $c_p T_0$ is defined as

$$\tau_\lambda = \frac{T_{t.AB}}{T_0} \tag{A.5}$$

where $T_{t.AB}$ is found using the application of the Chemical Equilibrium Analysis (CEA) software for fuel/oxidizer of hydrogen and oxygen. The fuel to air ratio f is then found using the steady flow energy equation (first law of thermodynamics) to the control volume about the afterburner as follows:

$$\dot{m}_e c_p T_{te} + \eta_b \dot{m}_f h_{PR} = (\dot{m}_e + \dot{m}_f) c_p T_{t.AB} \tag{A.6}$$

where h_{PR} is the value of the thermal energy released by the fuel during combustion and η_b is the burner efficiency, both of those values should be given. Dividing both sides by $\dot{m}_0 c_p T_0$ where $\dot{m}_0$ in this analysis is equal to $\dot{m}_s + \dot{m}_p$ and therefore with $\dot{m}_0 c_p T = \dot{m}_e c_p T_0$, we get the following equation:

$$\tau_r \tau_{ejec} + f \frac{\eta_b h_{PR}}{c_p T_0} = (1 + f)\tau_\lambda \tag{A.7}$$

Solving this equation for f we get the equation for fuel to air ratio

$$f = \frac{\tau_\lambda - \tau_r \tau_{ejec}}{h_{PR}/(c_{pc} T_e) - \tau_\lambda} \tag{A.8}$$

The total-to-static nozzle pressure ratio is given by

$$\frac{P_{t9}}{P_9} = \frac{P_0}{P_9}\frac{P_{t0}}{P_0}\frac{P_{ts}}{P_{t0}}\frac{P_{te}}{P_{ts}}\frac{P_{t.AB}}{P_{te}}\frac{P_{t9}}{P_{t.AB}} \tag{A.9}$$

where $\frac{P_{t0}}{P_0} = \pi_r$, $\frac{P_{ts}}{P_{t0}} = \pi_d$ its value is assumed from the ejector analysis. $\frac{P_{te}}{P_{ts}} = \pi_{ejec}$

$\frac{P_{t.AB}}{P_{te}} = \pi_b$, and finally $\frac{P_9}{P_{t.AB}} = \pi_n$

Using the nozzle pressure equation, the nozzle Mach number M_9 can then be found

$$M_9 = \sqrt{\frac{2}{\gamma - 1}\left[\left(\frac{P_{t9}}{P_9}\right)^{(\gamma-1)/\gamma} - 1\right]} \tag{A.10}$$

The nozzle static temperature ratio is then found to be

$$\frac{T_9}{T_0} = \frac{\tau_\lambda}{(P_{t9}/P_9)^{(\gamma-1)/\gamma}} \tag{A.11}$$

The equation of the engine Mach number is then found to be equal to:

$$\frac{V_9}{a_0} = M_9\sqrt{\frac{T_9}{T_0}} \tag{A.12}$$

The specific thrust equation is

$$\frac{F}{\dot{m}_0} = a_0\left[(1+f)\frac{V_9}{a_0} - M_0 + (1+f)\frac{T_9/T_0}{V_9/a_0}\frac{1 - P_0/P_9}{\gamma}\right] \tag{A.13}$$

The specific fuel consumption

$$S = \frac{f}{F/\dot{m}_0} \tag{A.14}$$

The thermal efficiency

$$\eta_T = \frac{{a_0}^2[(1+f)(V_9/a_0)^2 - M_0^2]}{2gfh_{PR}} \tag{A.15}$$

The propulsive efficiency

$$\eta_P = \frac{2gV_0(F/\dot{m}_0)}{{a_0}^2[(1+f)(V_9/a_0)^2 - M_0^2]} \tag{A.16}$$

REFERENCES

[1] Takuma, E. and Fujiwara, T., "A Simplified Analysis on a Pulse Detonation Engine Model," *Trans. Japan Soc. Aero. Space Sci.* Vol. 44, No. 146, 2002

[2] Heiser, W. and Pratt, D., *Hypersonic Airbreathing Propulsion*, AIAA, 1994

[3] Liepmann, H.W. and Roshko, A., *Elements of Gasdynamics,* Dover Publications, Inc. Meneola, NY, 2001.

[4] Mattingly, J. D., *Elements of Gas Turbine Propulsion*, McGraw-Hill, 1996

[5] Anderson, J. D., Jr. *Fundamentals of Aerodynamics*, third edition, McGraw-Hill, 2001.

[6] Daniel, E. P., Wilson, J. and Kelvin, T.D., "Unsteady Ejector Performance: An Experimental Investigation Using a Pulsejet Driver," AIAA 2002-3915, June 2002

[7] Bellini, R. and Lu, F.K., "Exergy Analysis of a Hybrid Pulse Detonation Power Device,"

[8] Santoro R.J., Lee S. Y, Saretto S., Shehadeh R.., "Experimental Study of Pulse Detonation Engine Driven Ejector.," AIAA 2002-4972, July 2003.

[9] Bussing, T. and Pappas, G., "An Introduction to Pulse Detonation Engines," AIAA 94-0263, January 1994.

[10] Sharma, S.D., Ahmed, M.R., "Effect of velocity ratio on the turbulent mixing of confined, co-axial jets," Elsevier Science Inc., 2000.

[11] Kailasanath, K., "Recent Developments in the Research on Pulse Detonation Engines," AIAA Journal, Vol. 41, No. 2, 2003, pp. 145-159.

[12] Yungster, S. and Perkins, H.D., "Multiple-Cycle Simulation of Pulse Detonation Engine Ejector," AIAA 2002-3630, October 2002.

[13] Gordon, S. and McBride, B.J., "Computer Program for Calculation of Complex Chemical Equilibrium Compositions, Rocket Performance, Incident and Reflected Shocks, and Chapman-Jouguet Detonations," NASA SP 273, 1976 (http://www.grc.nasa.gov/WWW/CEAWeb/)